University of Alberta

PRODUCTION DATA ANALYSIS OF TIGHT HYDROCARBON RESERVOIRS

by

Shahab Kafeel Siddiqui

A thesis submitted to the Faculty of Graduate Studies and Research
in partial fulfillment of the requirements for the degree of

Master of Science
in
Petroleum Engineering

Department of Civil and Environmental Engineering

©Shahab Kafeel Siddiqui
Fall 2012
Edmonton, Alberta

Permission is hereby granted to the University of Alberta Libraries to reproduce single copies of this thesis and to lend or sell such copies for private, scholarly or scientific research purposes only. Where the thesis is converted to, or otherwise made available in digital form, the University of Alberta will advise potential users of the thesis of these terms.

The author reserves all other publication and other rights in association with the copyright in the thesis and, except as herein before provided, neither the thesis nor any substantial portion thereof may be printed or otherwise reproduced in any material form whatsoever without the author's prior written permission.

Dedication

I dedicate my work to all those who have lovingly supported me throughout life and all its travails.

Abstract

Tight reservoirs stimulated by multistage hydraulic fracturing are commonly described by a dual porosity model. This work hypothesizes that the production data of some fractured horizontal wells (which contain reactivated natural fractures) may also be described by a triple porosity model. We test this hypothesis by extending the existing triple porosity models to develop an analytical procedure for determining the reservoir parameters. We derive the simplified equations for different regions of the rate-time plot including linear and bilinear flow regions.

The second part of this work focuses on analyzing production data of tight oil reservoirs. We plot rate-normalized pressure (RNP) versus material balance time (MBT) of two wells drilled in Cardium and Bakken formations. We observe a half-slope followed by a unit-slope in both cases. We hypothesize that the unit slope reflects the linear pseudosteady state (PSS) flow and develop a new model to analyze this boundary-dominated flow.

Acknowledgements

First, I want to give praises to Almighty Allah for sparing my life, continuously granting me His blessings and allowing me to successfully conclude this phase of my life.

I want to acknowledge my supervisor, Dr. Hassan Dehghanpour for being a mentor, supervisor and friend to me. I am honored to have worked with him. I am also eternally grateful to him.

I would also like to thank Dr. Juliana Leung and Dr. Ahmed Bouferguene for serving on my advisory committee and for their constructive feedback that helps making this work better.

I want to acknowledge the eternal support of my parents, Kafeel Alam and Farzana Kafeel, and my beloved wife, Zubaria.

I also would like to acknowledge the help of my friend, Afsar Ali for the informative discussion and contributions to this work.

In addition, I would like to express my gratitude to my friends, colleagues and the Petroleum Engineering department faculty and staff for making my time at University of Alberta a great experience.

Table of Contents

List of Tables

List of Figures

CHAPTER I
INTRODUCTION

Tight oil and shale gas reservoirs are considered “unconventional” resources, requiring horizontal wells and massive hydraulic fracturing for economic production. Tight hydrocarbon production is emerging as an important source of energy supply in the United States and Canada. Some of these unconventional resources are naturally fractured. A naturally fractured reservoir (NFR) can be defined as a reservoir that contains fractures (planar discontinuities) created by natural processes like diastrophism and volume shrinkage, distributed as a consistent connected network throughout the reservoir (Ordonez et al., 2001). Fractured petroleum reservoirs represent over 20% of the world's oil and gas reserves (Saidi, 1983).

Horizontal drilling and multi-stage fracture stimulation is a successful technique in allowing shale gas production. It has proved to work equally well for producing light crude oil trapped in low permeability (e.g., tight) shale, sandstone, or carbonate rock formations. Characterization and modeling of naturally fractured tight reservoirs stimulated by hydraulic fractures present unique challenges that differentiate them from conventional reservoirs.

Traditionally, dual-porosity models have been used to model NFRs where all fractures are assumed to have identical properties. Different dual-porosity models have been proposed such as Warren & Root (1963) sugar cube model in which matrix provides the storage while fractures provide the flow medium. The model assumed pseudosteady state fluid transfer between matrix and fractures. Since then, several models were developed mainly as variation of the Warren & Root model assuming different matrix- fracture fluid transfer conditions (Kazemi 1969 and Liu 1981).

Characterizing and modeling NFRs is challenging due to the highly heterogeneous and anisotropic nature of the fracture system (Ordonez et al., 2001). It is more realistic to assume fractures having different properties. This is more apparent in case of hydraulically fractured wells. Thus, triple-porosity model have been developed and is more realistic models to capture reservoir heterogeneity in hydraulically fractured NFRs. Triple porosity model developed for linear flow that considers transient fluid transfer (between media) is available in the literature (Al-Ahmadi, 2010). In this work we further extend this model to develop analysis equations of each flow regime observed during hydrocarbon production.

Furthermore, the existing models available in the literature are useful in analyzing matrix flow in hydraulically fractured reservoir. No appropriate models are available to analyze the boundary dominated linear flow. Boundary dominated flow in the hydraulically fractured reservoirs occurs when the pressure interference reaches the virtual no flow boundaries developed at the center of two adjacent fractures. New analysis equations are developed to model this flow occurring under pseudosteady state flow conditions.

1.1. PROBLEM DEFINITION

Horizontal wells with multistage hydraulic fracturing are used to produce economically from NFRs. It has been documented that hydraulic fractures growth could re-open the pre-existing natural fractures (Gale *et al.* 2007). Therefore, for any model to be used to analyze such wells, it has to account for both natural and hydraulic fractures to be practical. Under these conditions, the reservoir should be described by a triple porosity model.

1.2 OBJECTIVES

The objective of this research is to develop analysis equations to model each flow regime occurring during production from a horizontal well in a triple-porosity reservoir. The system consists of matrix and two sets of orthogonal fractures that have different properties. These fractures are the more permeable macro-fractures and the less permeable micro-fractures. Existing triple porosity model for linear systems will be extended. New analytical equations will also be derived to model boundary dominated flow in dual porosity reservoirs.

1.3 OUTLINE

This dissertation is divided into seven chapters. It is organized in a manner that follows a gradual process of developing a conceptual and logical understanding of the basic dual and triple porosity model and its limitations. It progresses through by developing the analysis equations of different flow regimes observed during production from a triple porosity system. This dissertation also includes the modeling of boundary dominated (pseudosteady state) flow for linear dual porosity reservoirs.

Chapter II presents a literature review of existing dual and triple porosity models and its extensions for linear flow. This chapter also includes review of existing models to analyze boundary dominated flow.

Chapter III discusses the new analysis equations developed for linear flow towards a horizontal well in triple porosity reservoirs. The new equations are developed to analyze each individual flow regime observed during hydrocarbon production. The solutions are presented for slightly compressible (oil) and highly compressible (gas) fluids.

Chapter IV presents the new equations are developed to model the boundary dominated (pseudosteady state) flow for slightly compressible fluids in a dual porosity system.

Chapter V presents the application of the newly developed triple porosity model for two shale gas wells.

Chapter VI presents the application of new equations developed in Chapter V for modeling boundary dominated flow for tight oil reservoirs. The transient linear matrix flow of tight oil reservoirs is also analyzed using previously developed dual porosity equations. The analysis results obtained from both models are compared.

Chapter VII presents conclusions and recommendations.

CHAPTER II
LITERATURE REVIEW

2.1 INTRODUCTION

This chapter provides the literature review of naturally fractured reservoirs. Some of available dual and triple porosity models will be reviewed. In addition, linear flow solutions for the fractured reservoirs will be discussed.

2.2 DUAL POROSITY MODELS

Dual porosity models are usually used to analyze naturally fractured reservoirs. These models assume fractures to have identical properties. Barenblatt et al. (1960) introduced the first dual porosity model. Warren and Root (1963) extended Barenblatt model for well test analysis. The model presented by Warren and Root forms the basis of modern day analysis of naturally fractured reservoirs (NFRs). The model assumes that the fluid transfer between matrix and fractures is under pseudosteady state. The fractures provide flow medium and matrix provide storage of fluid. They introduced two dimensionless parameters, storativity (ω) and interporosity flow parameter (λ).

Dual porosity models can be further categorized based on the interporosity fluid transfer assumptions:

i) Pseudosteady state models
ii) Transient models

2.2.1 Pseudosteady state models

Warren and Root (1963) analyzed NFRs by idealizing matrix blocks as sugar cubes and assumed a continuous uniform fracture network oriented parallel to the principal axes of permeability (**Fig 2.1**). They assumed pseudosteady flow between matrix and fracture system. In their model, two differential forms (one for matrix and one for fracture were solved simultaneously at a mathematical point. An equation for interporosity flow from the matrix to the fractures was presented:

$$q = \alpha \frac{k_m}{\mu} \left(P_m - P_f\right) \tag{2.1}$$

Where, q is the fluid transfer rate, α is the Warren and Root shape factor, P_m is the matrix pressure, P_f is the pressure of fractures, μ is the viscosity of fluid and k_m is the matrix permeability.

Warren and Root applied the Laplace transformation to obtain transfer function "$f(s)$" and presented a method to analyze pressure build up data for infinite radial reservoirs. Kazemi et al (1968) extended his model to interference testing.

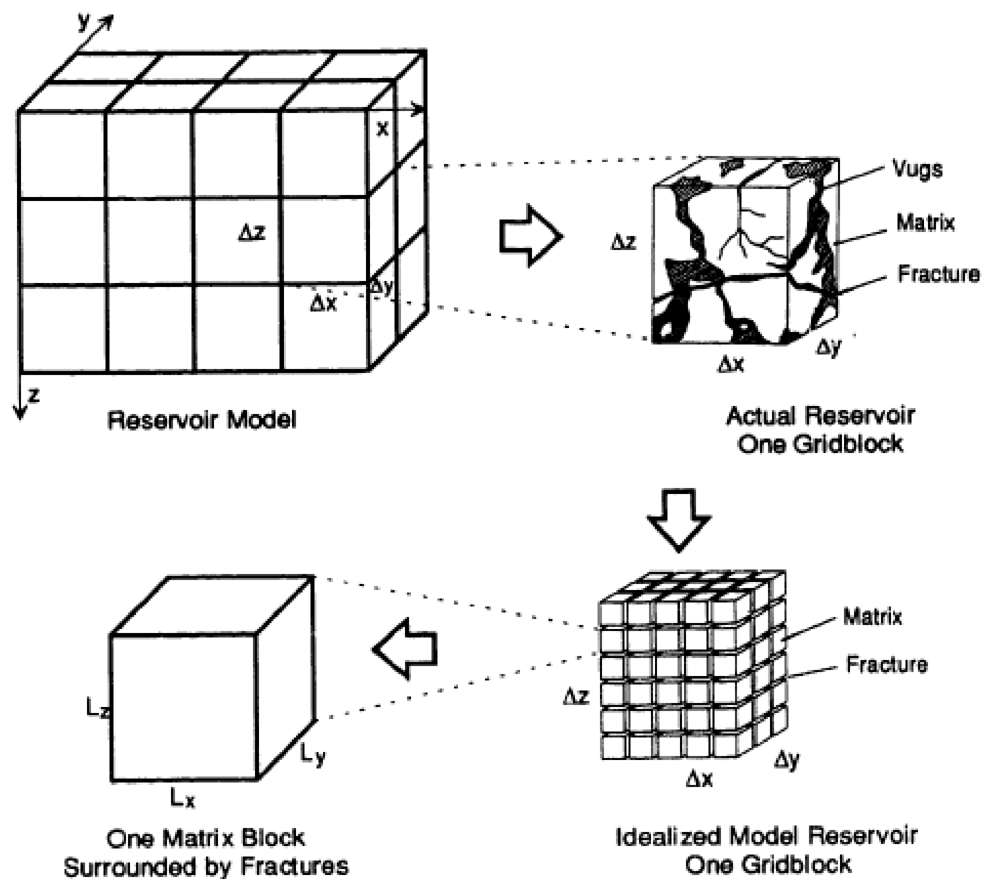

Fig. 2.1 – Idealization of the NFR system (Warren and Root, 1963).

Da Prat et al. (1981) extended the Warren and Root (1963) solutions to constant pressure inner boundary conditions and bounded outer boundary cases for radial reservoir and presented type curves for declined curve analysis.

2.2.2 Transient Models

Kazemi (1969) proposed a slab matrix model with horizontal fractures based on transient flow condition between matrix and fracture systems. The solutions were developed for single-phase flow in radial reservoirs. He solved the problem using numerical techniques. It was concluded that the results are similar to that of Warren and Root. Thus this model is also appropriate for analyzing NFRs.

2.3 Triple-porosity Models

The induced hydraulic fractures can create new fractures or reactivate the pre-existing natural fractures that may transform the reservoir into a triple porosity media (Gale et al 2007).

Liu (1981) introduced the first triple porosity model. The system consists of two matrix systems flowing into one fracture. The model was developed for radial flow of slightly compressible fluids. The interporosity flow in the reservoir is considered under pseudosteady state. This model was not published in petroleum literature.

Abdassah and Ershagi (1986) developed the first triple porosity model for petroleum literature. They developed an improved model for pressure transient tests of naturally fractured reservoirs. Geometrical configuration studied include, both the strata model and uniformly distributed blocks. Both models considered two matrix systems with different properties flowing under transient interporosity flow. It was concluded that the triple-porosity systems are characterized by anomalous slope changes during the matrix-flow controlled region. The slope change is the result of the contribution of matrix blocks that have the lowest interporosity flow.

Al-Ghamdi and Ershaghi (1996) introduced the concept of dual fracture triple porosity model. Dual fracture model consist of highly permeable macro fractures and less permeable micro fractures. They proposed two sub models to represent the dual fracture system. The first model is similar to the triple porosity system (two matrix systems and one fracture) where one of the matrix systems is replaced by micro-fractures. This model assumes no interporosity flow between the micro-fracture and the matrix systems, yet both support flow in the macro-fracture system. The second model assumes pressure support from the matrix to the micro-fractures, which in turns feed the macro-fractures. The macro-fractures and the micro-fractures both contribute to the production at the test well.

Liu et al. (2003) presented a mathematical model for analysis of pressure behavior in a tri-continuum medium. The medium consists of fractures, rock matrices and cavities. Fractures are considered to have homogeneous properties whereas matrix and cavities have different permeability and porosity. The matrix and cavities provide fluid storage and feeds the fractures and the fractures feeds the well. The interporosity flow occurs under pseudosteady state condition. The Warren–Root approach was used in developing the solution. The analytical model was applied to a published field-buildup test and was able to match the pressure buildup data.

Wu et al. (2004) proposed a triple-continuum model to study the effect of micro-fractures on flow and transport processes in fractured rocks to simulate the transport of tracers and nuclear waste of Yucca Mountain. They developed a triple-continuum system (consisting of large fractures, small fractures and matrix) for estimating reservoir parameters. They investigated the behavior of flow and transport processes in fractured rocks and verified the validity of analytical solutions with numerical modeling results. They concluded that the micro-fractures have a significant effect on the radionuclide transport in the system.

All the models previously described were developed for the radial reservoir cases.

2.4 LINEAR FLOW IN HYDRAULICALLY FRACTURED HORIZONTAL WELLS

Linear reservoirs are those reservoirs that show predominately linear flow because of the shape of reservoirs. These reservoirs would impose one-dimensional linear flow (El-Banbi 1998). Tight oil and gas reservoirs are hydraulically fractured through horizontal wells for economic production. Horizontal wells and hydraulically fractured horizontal wells may develop several linear flow periods depending on the type of well and shape of reservoirs. The duration of linear flow periods is governed by reservoir properties. Linear flow occurs at early times when the flow is perpendicular to any flow surface. Many wells have been observed to show long-term linear flow. Linear flow may be present for years before any boundary effects are reached. Several causes of linear transient flow may include draining of adjacent tight layers into high permeability layers, early-time constant pressure drainage and hydraulic fracture draining a square geometry (Wattenbarger, 2007).

Several authors (Miller, 1962 and Nabor and Barham, 1964) considered a linear reservoir model of rectangular geometry and presented constant rate and constant pressure solutions for linear aquifers.

El-Banbi (1998) was the first to present the analytical solution to model fluid flow in linear fractured reservoirs. New solutions were presented for naturally fractured reservoir using a linear reservoir model for dual porosity systems. Solutions are derived in Laplace domain for different inner boundary (constant pressure and constant rate) and outer boundary (infinite, closed and constant pressures). The effects of skin and wellbore storage effects have also been included.

Bello (2009) used El-Banbi solutions to model linear flow in dual porosity models. Horizontal well performance in tight fractured reservoirs was analyzed. El-Banbi's solution for constant pressure solution was applied to analyze rate transient in horizontal multi-stage fractured wells. He considered a bounded rectangular reservoir with slab matrix blocks draining into adjoining fractures and subsequently to a horizontal well in the center. Five flow regions were identified. New analytical equations for transient flow conditions were presented. Skin effect for the constant rate and constant pressure was also studied. His analytical equations for dual porosity transient linear will be used in this work to analyze wells exhibiting dual porosity behavior. Bello (2009) and Bello and Wattenbarger (2008, 2009, 2010) used the dual porosity linear flow model to analyze shale gas wells.

Al-Ahmadi (2010) extended Bello's (2009) dual porosity model and proposed a triple porosity model for horizontal fractured wells. This model assumes that micro fractures are perpendicular to the hydraulic fractures and parallel to the horizontal well. The model was developed based on the assumption that the flow is sequential from the matrix to the micro fractures and from the micro fractures to the hydraulic fractures and no flow occurs between matrix and hydraulic fractures. Four sub-models were developed based on the interporosity flow assumptions for transient and pseudosteady state flow conditions. He presented fracture transfer function "$f(s)$" for all four models. Non-linear regression analysis technique was used to calculate the unknown reservoir parameters for hydraulically fractured shale gas horizontal well.

Dehghanpour and Shirdel (2011) developed the triple porosity model for inner shale reservoir (**Fig 2.2**). The system consists of macro fractures with higher permeability, matrix blocks with intermediate permeability and porosity and matrix blocks with low permeability and porosity. They extended the existing dual porosity models and studied the pressure response under transient and pseudosteady state condition. They also performed sensitivity analysis to study the effect of properties of each medium on the pressure response.

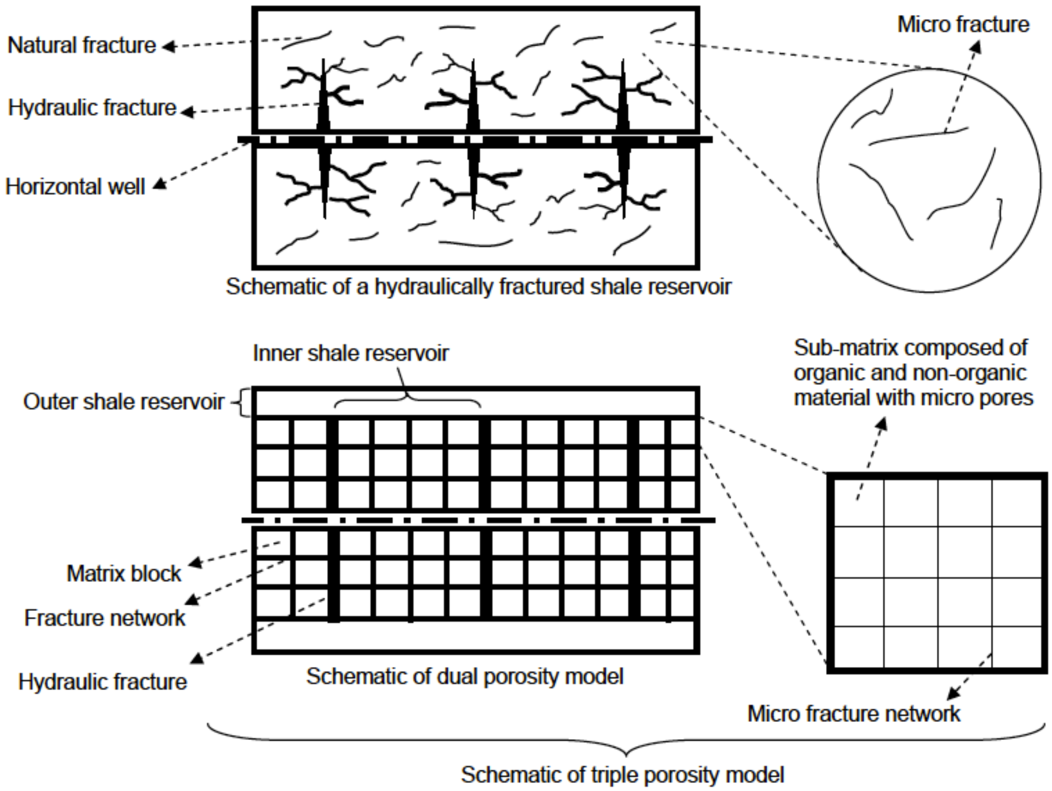

Fig. 2.2 – Schematic illustration of triple porosity model (Dehghanpour and Shirdel, 2011)

In this work Al-Ahmadi's transfer function is further simplified for the transient case only and analytical equations are developed and presented to characterize triple porosity reservoirs.

2.5 Boundary Dominated (Pseudosteady state) Flow

After the transient matrix flow in linear reservoirs, boundary dominated flow occurs. This flow is under pseudosteady state flow condition. This flow occurs as the pressure transient response reaches the virtual no flow boundaries developed between two adjacent hydraulic fractures.

Blasingame and Lee (1986) introduced the original analysis equation for boundary-dominated flow (i.e. pseudo steady state flow) for radial reservoirs.

Placio and Blasingame (1993) later modified their analysis equation for any instantaneous production time, flow regime or production scenario.

A new model for boundary dominated flow occurring in linear dual porosity reservoirs is developed in this work.

CHAPTER III

DEVELOPMENT OF ANALYSIS EQUATIONS FOR SEQUENTIAL TRIPLE POROSITY SYSTEM

3.1 INTRODUCTION

In this chapter, we develop the new analytical equations to analyze different flow regions observed on a rate-time plot of triple porosity system. This work is an extension of Al-Ahmadi's (2010) triple porosity model for transient linear flow. The triple porosity system consists of macro-fractures (higher permeability), micro fractures (intermediate permeability) and matrix (low permeability). The matrix feeds only the micro-fractures and micro-fractures feeds the macro-fractures. The macro-fractures are connected to horizontal well. The model and analysis equation are developed based on the assumption that the flow is sequential from one medium to another.

3.2 TRIPLE-POROSITY MODEL FOR SEQUENTIAL LINEAR FLOW

Al-Ahmadi (2010) proposed a new triple porosity model to analyze linear flow in a triple porosity system. A schematic of the triple porosity model is shown in Fig 3.1. The arrows indicate the flow direction. The fluid flows from the matrix to the micro-fractures and then to the macro-fractures and finally to the horizontal well. This model is an extension to the transient dual porosity model proposed by Kazemi (1969). Al-Ahmadi made the following assumptions to develop the analytical solutions.

1. The closed rectangular reservoir is producing at a constant rate through a horizontal well centrally placed in the reservoir
2. Triple porosity system consists of three contiguous media i.e. matrix, micro-fractures and macro fractures
3. Each media in the reservoir is assumed to be homogenous and isotropic
4. Matrix blocks are idealized as slabs

5. Flow direction is sequential
6. Fluid is slightly compressible

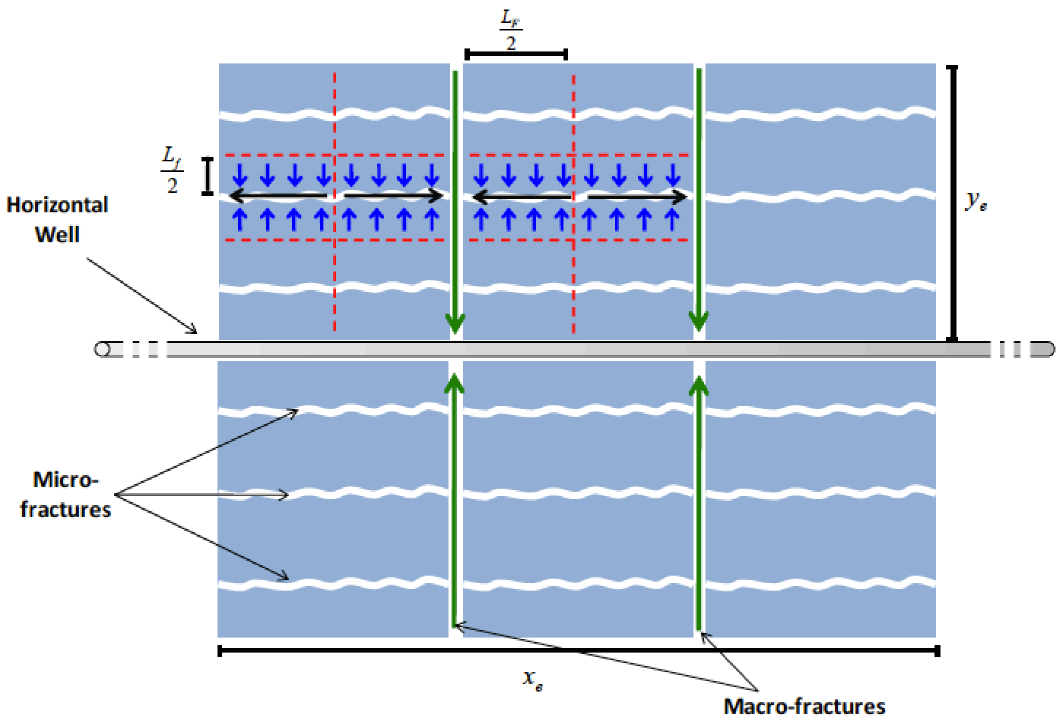

Fig. 3.1 – Top view of a horizontal well in a triple porosity system. Red dotted lines indicated virtual no flow boundaries. Arrows indicate direction of the flow (Al-Ahmadi 2010).

El-Banbi (1998) presented the constant rate and constant pressure solutions for linear fluid flow in fractured reservoirs. The analytical solution in Laplace domain for the constant rate is given by

$$\frac{1}{q_{Dl}} = \frac{2\pi s}{\sqrt{sf(s)}}\left[\frac{1+e^{-2\sqrt{sf(s)}y_{De}}}{1-e^{-2\sqrt{sf(s)}y_{De}}}\right] \tag{3.1}$$

Al-Ahmadi (2010) derived the new transfer functions that can be used in Eq. 3.1 to model triple porosity systems. He proposed four sub-models of the triple porosity system for pseudosteady state and transient flow conditions. The fracture functions $f(s)$ for the fully transient triple porosity model in Laplace domain are given by

$$f(s) = \omega_F + \frac{\lambda_{AcFf}}{3s}\sqrt{sf_f(s)}\,tanh\,\sqrt{sf_f(s)} \tag{3.2}$$

Where $f_f(s)$ is given by

$$f_f(s) = \frac{3\omega_f}{\lambda_{AcFf}} + \frac{\lambda_{Acfm}}{s\lambda_{AcFf}}\sqrt{\frac{3s\omega_m}{\lambda_{Acfm}}}\,tanh\,\sqrt{\frac{3s\omega_m}{\lambda_{Acfm}}} \tag{3.3}$$

The dimensionless variables is Eq. 3.1, 3.2 and 3.3 are defined as

$$\frac{1}{q_{Dl}} = \frac{k_F\sqrt{A_{cw}}\left[m(p_i) - m\left(p_{wf}\right)\right]}{1422q_gT} \tag{3.4}$$

$$t_{dac} = \frac{0.00633k_Ft}{(\emptyset\mu c_t)_tA_{cw}} \tag{3.5}$$

$$\lambda_{AcFf} = \frac{12}{{L_F}^2}\frac{k_f}{k_F}A_{cw} \tag{3.6}$$

$$\lambda_{Acfm} = \frac{12}{{L_f}^2}\frac{k_m}{k_F}A_{cw} \tag{3.7}$$

$$\omega_i = \frac{(\emptyset\mu c_t)_i}{(\emptyset\mu c_t)_t} \tag{3.8}$$

Where *i*= *F*, *f and m*,

$$(\emptyset\mu c_t)_t = (\emptyset\mu c_t)_F + (\emptyset\mu c_t)_f + (\emptyset\mu c_t)_m \tag{3.9}$$

$$y_{De} = \frac{y}{\sqrt{A_{cw}}} \tag{3.10}$$

$$z_D = \frac{z}{L_f/_2} \tag{3.11}$$

$$x_D = \frac{x}{L_F/_2} \tag{3.12}$$

Refer to Appendix A for a detailed derivation of this linear triple porosity model.

3.3 Flow Regions Based on the Analytical Solution

There are six different region identified by Al-Ahmadi (2010) for the constant pressure solution as the pressure propagates through the triple porosity system. The solutions are obtained by replacing Eq. 3.2 and 3.3 in Eq. 3.1. These solutions are inverted to real (time) domain using inverting algorithms like Stehfest Algorithm (Stehfest 1970). The solutions are then plotted on a log-log plot of dimensionless flow rate versus dimensionless time. **Figure 3.2** shows different flow regimes observed during production.

A negative quarter-slope identifies the bi-linear transient flow region and a negative half-slope identifies the linear transient flow region. Region 1 represents the linear flow through the hydraulic fractures. Region 2 represents the bi-linear flow due to simultaneous depletion of macro fractures and micro fractures.

Region 3 represents the linear flow through micro fractures. Region 4 represents bi-linear flow due to simultaneous depletion of the micro- fractures and the matrix blocks. Region 5 is the linear flow from matrix blocks. Region 6 represents the boundary dominated flow.

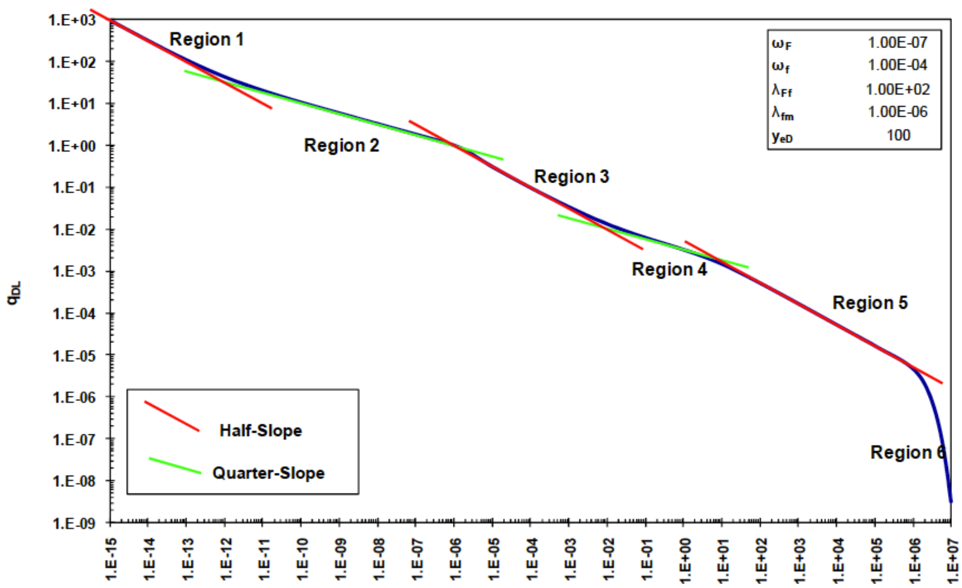

Fig. 3.2 – Log-log plot of dimensionless rate versus dimensionless time for a triple porosity system. Bi-linear flow indicated by a slope of 0.25 and linear flow is indicated by slope of 0.5 (Al Ahmadi 2010).

3.4 Development of Analysis Equation for Flow Regions Observed During Production

In this work we further simplify Eq. 3.2 and Eq. 3.3 to develop the new equations to analyze each flow region observed during production. We develop the analysis equation for the triple porosity system for transient case only. Bello (2009) developed similar analytical equations to analyze rate transient in horizontal multi-stage fractured shale gas wells for dual porosity system.

The details of the derivation are shown in Appendix B.

3.4.1 Region 1

We observe this region when transient linear flow occurs in macro-fractures. This occurs at early time scales when the drainage of micro-fractures and matrix is negligible. A negative half-slope on the log-log plot characterizes this region. We simplify Eq. 3.2 and 3.3 to obtain a dimensionless equation to analyze this region. The mathematical details are given in Appendix B-1. The equation for Region 1 is given by

$$q_{Dl} = \frac{1}{2\pi\sqrt{\pi t_{dac}}}\sqrt{\omega_f} \tag{3.13}$$

Equation 3.13 can be converted into dimensional form by substituting dimensionless parameters defined by Eq. 3.4 to Eq. 3.12:

$$\sqrt{k_F}A_{cw} = \frac{1262T}{\sqrt{(\emptyset\mu c_t)_f}}\frac{1}{m_1} \tag{3.14}$$

Where m_1 is the slope obtained by plotting $\frac{m(p_i)-m(p_{wf})}{q_g}$ versus $\sqrt{t}$. We can calculate the permeability of macro-fractures using Eq. 3.14 if the other parameters are known.

A_{cw} is the total drainage area of the reservoir and can be calculated by

$$A_{cw} = 2 \times X_e \times h \tag{3.15}$$

3.4.2 Region 2

We observe this region during simultaneous depletion of both macro-fracture and micro-fracture (bi-linear flow). This region is characterized by a negative quarter-slope on the log-log plot. We simplify Eq. 3.2 and 3.3 to obtain a dimensionless equation to analyze this region. The mathematical details are given in Appendix B-2. The dimensionless equation for Region 2 is given by

$$q_{Dl} = \frac{1}{10.1332} \sqrt[4]{\frac{\lambda_{AcFf}\omega_f}{t_{dac}}} \tag{3.16}$$

Equation 3.16 can be converted into dimensional form by substituting dimensionless parameters defined by Eq. 3.4 to Eq. 3.12:

$$\sqrt{k_F} A_{cw} = \frac{4070T}{\sqrt[4]{\sigma_F k_f (\text{Ø}\mu c_t)_f}} \frac{1}{m_2} \tag{3.17}$$

Where m_2 is the slope obtained by plotting $\frac{m(p_i) - m(p_{wf})}{q_g}$ versus $\sqrt[4]{t}$. If Region 2 is observed and other parameters are known, Eq. 3.17 can be used to determine $k_F\sqrt{k_f}$.

3.4.3 Region 3

We observe this region when transient linear flow occurs in micro-fracture. A negative half-slope on the log-log plot characterizes this region. We simplify Eq. 3.2 and 3.3 to obtain a dimensionless equation to analyze this region. The mathematical details are given in Appendix B-3. The dimensionless equation for Region 3 is given by

$$q_{Dl} = \frac{1}{2\pi\sqrt{\pi t_{dac}}} \sqrt{\frac{\lambda_{AcFf}\omega_f}{3}} y_{De} \tag{3.18}$$

Equation 3.18 can be converted into dimensional form by substituting dimensionless parameters defined by Eq. 3.4 to Eq. 3.12:

$$\sqrt{\sigma_F}y_e\sqrt{k_f}A_{cw} = \frac{2182T}{\sqrt{(\emptyset\mu c_t)_f}}\frac{1}{m_3} \tag{3.19}$$

Where $\sigma_F = \frac{12}{{L_F}^2}$ (3.20)

Where m_3 is the slope obtained by plotting $\frac{m(p_i)-m(p_{wf})}{q_g}$ versus $\sqrt{t}$. If Region 3 is observed and other parameters are known, Eq. 3.19 can be used to determine k_f or y_e if one is known from other sources.

3.4.4 Region 4

We observe this region when both matrix and micro-fracture deplete at the same time. A negative quarter slope on the log-log plot characterizes this region. We simplify Eq. 3.2 and 3.3 to obtain a dimensionless equation to analyze this region. The mathematical details are given in Appendix B-4. The dimensionless equation for Region 4 is given by

$$q_{Dl} = \frac{1}{17.31}\sqrt{\lambda_{AcFf}}\sqrt[4]{\frac{\lambda_{Acfm}\omega_m}{t_{dac}}}y_{De} \tag{3.21}$$

Equation 3.21 can be converted into dimensional form by substituting dimensionless parameters defined by Eq. 3.4 to Eq. 3.12:

$$\sqrt{\sigma_F} y_e \sqrt{k_f} A_{cw} = \frac{6943T}{\sqrt[4]{\sigma_f k_m (\text{Ø}\mu c_t)_m}} \frac{1}{m_4} \tag{3.22}$$

Where $\sigma_f = \frac{12}{{L_f}^2}$ (3.23)

Substituting shape factor σ_f in Equation 3.22

$$\sqrt{\sigma_F} y_e \sqrt{\frac{k_f}{L_f}} A_{cw} = \frac{2004T}{\sqrt[4]{k_m (\text{Ø}\mu c_t)_m}} \frac{1}{m_4} \tag{3.24}$$

Where m_4 is the slope obtained by plotting $\frac{m(p_i)-m(p_{wf})}{q_g}$ versus $\sqrt[4]{t}$. If Region 4 is observed and other parameters are known, Eq. 3.24 can be used to determine the ratio $\frac{k_f}{L_f}$, if y_e is known from other sources.

3.4.5 Region 5

We observe this region when transient linear flow occurs in matrix. This is the longest region we observe before reaching the boundary effect. A negative half-slope on the log-log plot characterizes this region. Analysis of this region gives the total matrix drainage area that determines the effectiveness of stimulation job. We simplify Eq. 3.2 and 3.3 to obtain a dimensionless equation to analyze this region. The mathematical details are given in Appendix B-5. The dimensionless equation for Region 5 is given by

$$q_{Dl} = \frac{1}{2\pi\sqrt{\pi t_{dac}}} \sqrt{\frac{\lambda_{Acfm}\omega_m}{3}}\, y_{DE} \tag{3.25}$$

Equation 3.25 can be converted into dimensional form by substituting dimensionless parameters defined by Eq. 3.4 to Eq. 3.12:

$$\sqrt{\sigma_F}y_e\sqrt{k_m}A_{cw} = \frac{2182T}{\sqrt{(\emptyset\mu c_t)_m}}\frac{1}{m_5} \tag{3.26}$$

Where m_5 is the slope obtained by plotting $\frac{m(p_i)-m(p_{wf})}{q_g}$ against $\sqrt{t}$. We can calculate the stimulated fracture half-length y_e by analyzing this region.

A_{cm} is the area of interface between matrix and micro fractures (for triple porosity case) and is given by

$$A_{cm} = A_{cw}\frac{2\,y_e}{L_f} \tag{3.27}$$

Here,

A_{cw} is the drainage area given by Eq. 3.15

y_e is the fracture half-length.

L_f is the spacing between micro fractures

Where $\frac{y_e}{L_f}$ represents the number of micro fractures (n_{fye}).

Therefore, Eq. 3.26 can be converted to simpler form

$$\sqrt{k_m}A_{cm} = \frac{2182T}{\sqrt{(\emptyset\mu c_t)_m}}\frac{1}{m_5} \tag{3.28}$$

If Region 5 is observed and other parameters are known, Eq. 3.28 can be used to determine the matrix drainage area A_{cm}.

3.4.6 Region 6

We observe this region when the reservoir boundary begins to influence the transient response. In other words, the pressure transient response in the matrix blocks has reached the virtual no flow boundaries developed between two adjacent fractures. This region is also defined in the petroleum literature as boundary dominated flow. We can calculate the stimulated reservoir volume SRV by analyzing this region to estimate the OOIP and OGIP. We will derive an equation for boundary-dominated flow of slightly compressible fluid in linear dual porosity system.

The summary of the results for the highly compressible fluids (gas) and slightly compressible fluid (oil) is presented in Table 3.1 and Table 3.2 respectively.

Table 3.1 Summary of analysis equations developed for constant P_{wf} of rate transient solution for triple porosity system for highly compressible fluid (gas)		
Region	**Inverse Laplace Solution**	**Analysis Equation**
Region 1 (Macro-Fracture Flow)	$q_{DL} = \frac{1}{2\pi\sqrt{\pi t_{dac}}}\sqrt{\omega_f}$	$\sqrt{k_F}A_{cw} = \frac{1262T}{\sqrt{(\emptyset\mu c_t)_F}}\frac{1}{m_1}$
Region 2 (Bilinear flow b/w macro & micro-fractures)	$q_{DL} = \frac{1}{10.133}\sqrt[4]{\frac{\lambda_{AcFf}\omega_f}{t_{dac}}}$	$\sqrt{k_F}A_{cw} = \frac{4070T}{\sqrt[4]{\sigma_F k_f(\emptyset\mu c_t)_f}}\frac{1}{m_2}$
Region 3 (Micro-fracture flow)	$q_{DL} = \frac{1}{2\pi\sqrt{\pi t_{dac}}}\sqrt{\frac{\lambda_{AcFf}\omega_f}{3}}y_{De}$	$\sqrt{\sigma_F}y_e\sqrt{k_f}A_{cw} = \frac{2182T}{\sqrt{(\emptyset\mu c_t)_f}}\frac{1}{m_3}$
Region 4 (Bilinear flow b/w matrix & micro-fractures)	$q_{DL} = \frac{1}{17.54}\sqrt{\lambda_{AcFf}}\sqrt[4]{\frac{\lambda_{Acfm}\omega_m}{t_{dac}}}y_{De}$	$\sqrt{\sigma_F}y_e\sqrt{\frac{k_f}{L_f}}A_{cw} = \frac{2004T}{\sqrt[4]{k_m(\emptyset\mu c_t)_m}}\frac{1}{m_4}$
Region 5 (Matrix flow)	$q_{DL} = \frac{1}{2\pi\sqrt{\pi t_{dac}}}\sqrt{\frac{\lambda_{Acfm}\omega_m}{3}}y_{De}$	$\sqrt{k_m}A_{cm} = \frac{1262T}{\sqrt{(\emptyset\mu c_t)_m}}\frac{1}{m_5}$

Table 3.2 Summary of analysis equations developed for constant P_{wf} of rate transient solution for triple porosity system for slightly compressible fluid (oil)

Region	**Inverse Laplace Solution**	**Analysis Equation**
Region 1 (Macro-fracture flow)	$q_{DL} = \frac{1}{2\pi\sqrt{\pi t_{dac}}}\sqrt{\omega_f}$	$\sqrt{k_F}A_{cw} = \frac{125.11 B_o \mu}{\sqrt{(\emptyset\mu c_t)_F}}\frac{1}{m_1}$
Region 2 (Bilinear flow b/w macro & micro-fractures)	$q_{DL} = \frac{1}{10.133}\sqrt[4]{\frac{\lambda_{AcFf}\omega_f}{t_{dac}}}$	$\sqrt{k_F}A_{cw} = \frac{403.5 B_o \mu}{\sqrt[4]{\sigma_F k_f (\emptyset\mu c_t)_f}}\frac{1}{m_2}$
Region 3 (Micro-fracture flow)	$q_{DL} = \frac{1}{2\pi\sqrt{\pi t_{dac}}}\sqrt{\frac{\lambda_{AcFf}\omega_f}{3}}y_{De}$	$\frac{L_f}{L_F}\sqrt{k_f}A_{cm} = \frac{125.11 B_o \mu}{\sqrt{(\emptyset\mu c_t)_f}}\frac{1}{m_3}$
Region 4 (Bilinear flow b/w matrix & micro-fractures)	$q_{DL} = \frac{1}{17.54\sqrt{\lambda_{AcFf}}}\sqrt[4]{\frac{\lambda_{Acfm}\omega_m}{t_{dac}}}y_{De}$	$\frac{L_f}{L_F}\sqrt{k_f}A_{cm} = \frac{403.5 B_o \mu}{\sqrt[4]{\alpha_m k_m (\emptyset\mu c_t)_m}}\frac{1}{m_4}$
Region 5 (Matrix flow)	$q_{DL} = \frac{1}{2\pi\sqrt{\pi t_{dac}}}\sqrt{\frac{\lambda_{Acfm}\omega_m}{3}}y_{De}$	$\sqrt{k_m}A_{cm} = \frac{125.11\ B_o \mu}{\sqrt{(\emptyset\mu c_t)_m}}\frac{1}{m_5}$

CHAPTER IV
DEVELOPMENT OF ANALYSIS EQUATION OF BOUNDARY DOMINATED FLOW

4.1 INTRODUCTION

In this chapter, we develop a new model for analyzing boundary dominated flow in fractured tight oil wells. In Chapter VI we use this model to analyze the boundary dominated flow in fractured tight oil reservoirs. The boundary dominated flow occurs under pseudosteady state flow conditions.

4.2 MODELING BOUNDARY DOMINATED FLOW IN FRACTURED HORIZONTAL WELLS

Pseudosteady state flow is observed when pressure interference occurs between two adjacent transverse fractures. A no flow imaginary boundary is formed at the middle of two adjacent fractures. We develop the equations to analyze this pseudosteady behavior identified by a unit-slope on the plot of rate-normalized pressure (RNP) versus material balance time (MBT). **Fig. 4.1** shows the no flow boundaries developed at the center of the matrix blocks separated by two adjacent fractures. A 3D view of the horizontal well placed in the center of reservoir is shown in **Fig. 4.2.**

4.2.1 Model Assumptions

In order to develop the analysis equations, we make the following assumptions:

1. The system is a dual porosity and no micro fractures (natural fractures) exist
2. The fluid flow is only from the matrix blocks to the hydraulic fractures and only hydraulic fractures feed the well bore
3. The fluid is slightly compressible and single phase
4. The no flow boundary is assumed to be in the middle of the matrix blocks separating two adjacent fractures
5. Spacing between the hydraulic fractures is uniform

6. When the pseudo steady state is reached, the pressure drop in the fractures is negligible
7. The contribution of the matrix blocks beyond the fracture half-length is ignored
8. Horizontal permeability is higher than vertical permeability

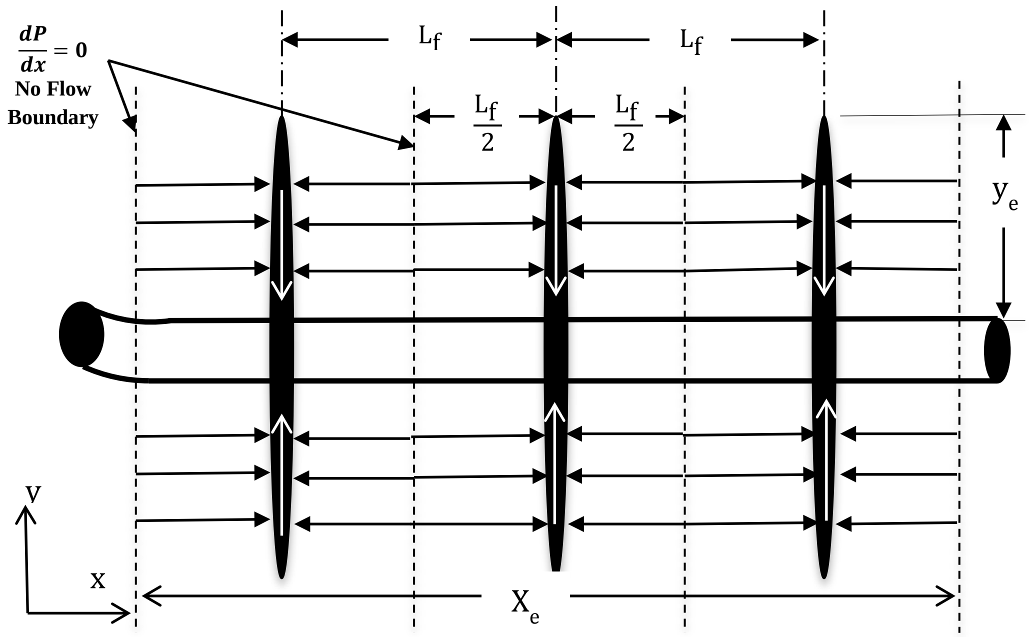

Fig. 4.1 – Plan view of hydraulic fractures connected to the horizontal well. The direction of flow is from the matrix to the fractures and from the fractures to the well. This figure also shows fracture half-length y_e. Arrows indicate the flow direction.

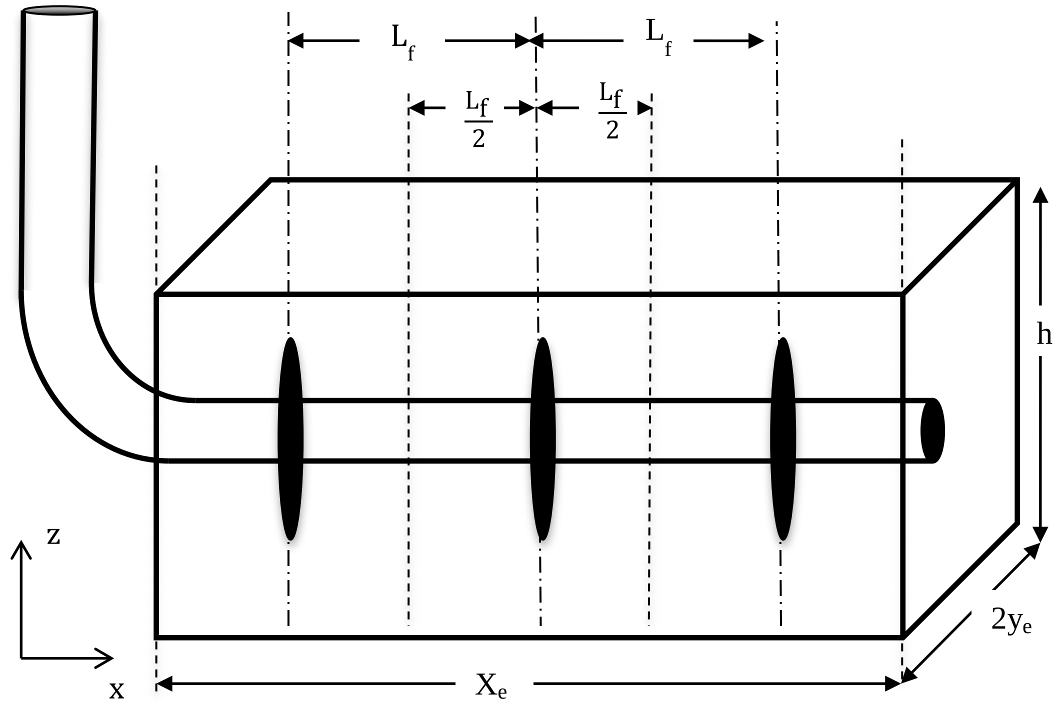

Fig. 4.2 – Front view of hydraulic fractures connected to the horizontal well.

4.3.2 Development of a New Solution for the Boundary Dominated Linear Flow in Horizontally Fractured Tight Reservoirs

Starting from the material balance equation and using the linear diffusivity equation, we model the boundary dominated linear flow in fractured tight reservoirs. To develop the analysis equation we consider, a control volume, V_m, shown in **Fig 4.3**. It represents the volume of reservoir feeding one fracture. The no-flow boundary is established at a distance of 0.5 L_f from the fracture where L_f is the spacing between the fractures.

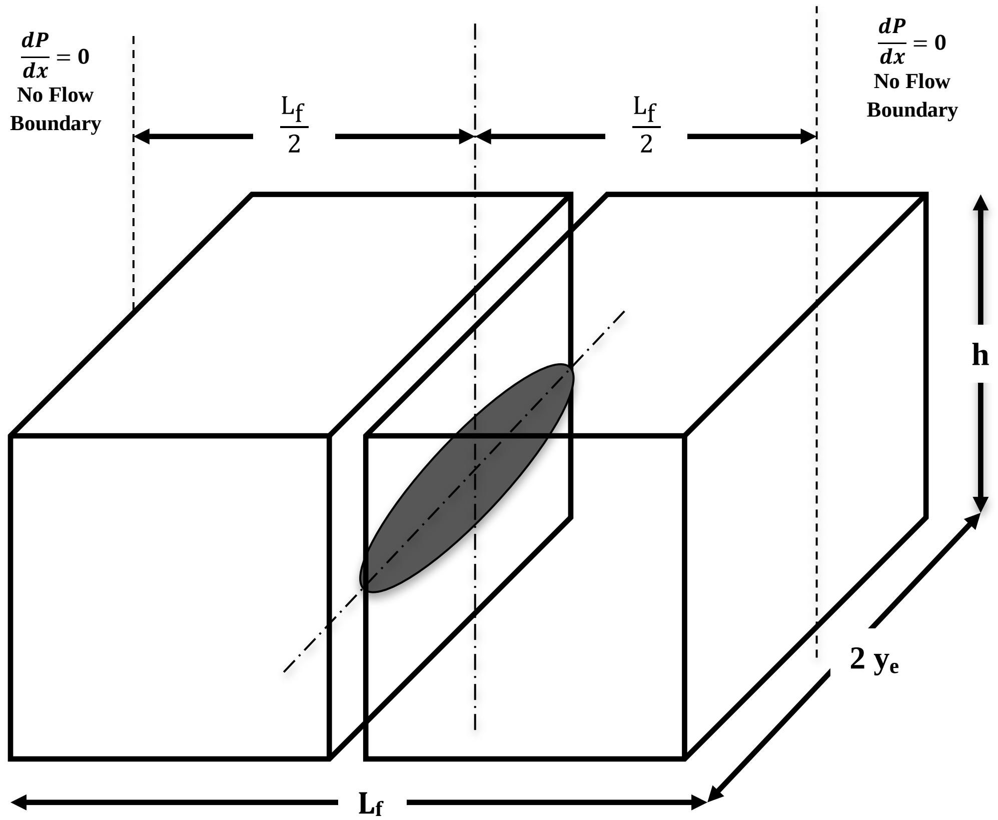

Fig. 4.3 – Schematic of the selected control volume showing a hydraulic fracture surrounded by the matrix blocks. Two no-flow boundaries are virtually created at the center of adjacent fractures at distance of 0.5 Lf from the fracture

We apply mass balance for control volume V_m as shown in Fig. 4.3,

4.3.2.1 Material balance equation

Mass in – Mass out = Accumulation in the matrix (4.1)

$$0 - q_o \rho_o \Delta t \big|_x = \rho_o \phi_m V_m \big|_{t+\Delta t} - \rho_m \phi_m V_m|_t \tag{4.2}$$

$$0 - q_o \rho_o = \frac{\rho_o \phi_m V_m \big|_{t+\Delta t} - \rho_m \phi_m V_m|_t}{\Delta t} \tag{4.3}$$

Taking limits as Δt approaches to zero

$$- q_o\rho_o = \frac{d}{dt}(\rho_o\ \phi_m V_m) \quad (4.4)$$

$$\frac{- q_o\rho_o}{V_m} = \frac{d}{dt}(\rho_o\ \phi_m) \quad (4.5)$$

Using chain rule

$$\frac{- q_o\rho_o}{V_m} = \frac{dP}{dt}\left(\phi_m \frac{d}{dP}\rho_o + \rho_o \frac{d}{dP}\phi_m\right) \quad (4.6)$$

Dividing both sides by ϕ_m and ρ_o

$$\frac{- q_o}{V_m\ \phi_m} = \frac{dP}{dt}\left(\frac{1}{\rho_o}\frac{d}{dP_m}\rho_o + \frac{1}{\phi_m}\frac{d}{dP}\phi_m\right) \quad (4.7)$$

$$\frac{- q_o}{V_m\ \phi_m} = \frac{dP}{dt}(\ c_w + \ c_f\ ) \quad (4.8)$$

$$\frac{- q_o}{V_m\phi_m} = \frac{dP}{dt}(\ c_t\ ) \quad (4.9)$$

$$\frac{dP}{dt} = -\frac{q_o}{V_m\phi_m\ c_t} \quad (4.10)$$

Where V_m is the controlled volume given by

$$V_m = L_f\ .h\ .2y_e \quad (4.11)$$

4.3.2.2 Linear Diffusivity Equation

Diffusivity equation for linear flow is given as

$$\frac{d^2P}{dx^2} = \left(\frac{\phi_m\ \mu_o\ c_t}{k_m}\right)\frac{dP}{dt} \quad (4.12)$$

Replacing $\frac{dP}{dt}$ from Eq. 4.9

$$\frac{d^2P}{dx^2} = \left(\frac{\phi_m\ \mu_o\ c_t}{k_m}\right)\left(-\frac{q_o}{V_m\phi_m\ c_t}\right) \quad (4.13)$$

Integrating both sides gives

$$\frac{dP}{dx} = \left(\frac{\mu_o}{k_m}\right)\left(-\frac{q_o}{V_m}\ x\right) + C1 \qquad (4.14)$$

Applying the first boundary condition

At $x = \frac{L_f}{2}, \frac{dP}{dx} = 0$

C1 is given by

$$C1 = \left(\frac{\mu_o}{k_m}\frac{q_o}{V_m}\right)\frac{L_f}{2} \qquad (4.15)$$

Replacing C1 from Eq. 4.15 into Eq. 4.14, we obtain

$$\frac{dP}{dx} = \left(\frac{\mu_o}{k_m}\right)\left(-\frac{q_o}{V_m}\ \right)x + \left(\frac{\mu_o}{k_m}\frac{q_o}{V_m}\right)\ \frac{L_f}{2} \qquad (4.16)$$

Integrating both sides of Eq. 4.16

$$\int dP = \int \left(\frac{\mu_o}{k_m}\right)\left(-\frac{q_o}{V_m}\right)x\ dx + \int \left(\frac{\mu_o}{k_m}\frac{q_o}{V_m}\right)\frac{L_f}{2}\ dx \qquad (4.17)$$

$$P_m = \left(\frac{\mu_o}{k_m}\right)\left(-\frac{q_o}{2\ V_m}\ x^2\right) + \left(\frac{\mu_o}{k_m}\frac{q_o}{V_m}\right)\frac{L_f}{2}x + C2 \qquad (4.18)$$

Applying the second boundary condition

At $x = 0, P_m = P_f$

Eq. 4.18 becomes

$$\mathrm{C2} = P_f \qquad (4.19)$$

Replacing C2 from Eq. 4.19 into Eq.4.18

$$P_m = \left(\frac{\mu_o}{k_m}\right)\left(-\frac{q_o}{2\ V_m}\ x^2\right) + \left(\frac{\mu_o}{k_m}\frac{q_o}{V_m}\right)\frac{L_f}{2}x + P_f \qquad (4.20)$$

Eq. 4.20 represents pressure profile in the matrix block.

4.3.2.3 Average matrix pressure from the pressure solution

Average pressure of the control volume V_m is given by

$$\overline{P_m} = \frac{\int_0^{\frac{L_f}{2}} P_m dV_m}{\int_0^{\frac{L_f}{2}} dV_m} \tag{4.21}$$

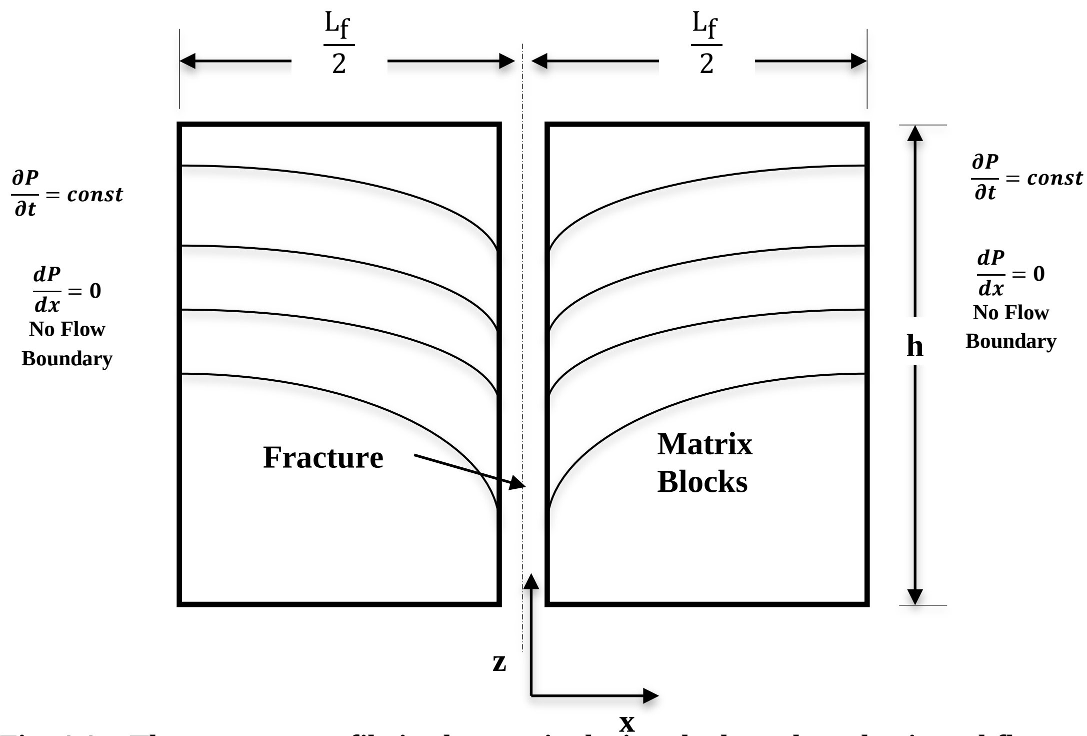

Fig. 4.4 – The pressure profile in the matrix during the boundary dominated flow. The rate of pressure drop with respect to time remains constant at pseudosteady state conditions.

Replacing P_m from Eq. 4.20 and

$$dV_m = 2\, ye \times h \times dx \tag{4.22}$$

On solving Eq. 4.21, the average matrix pressure is given by

$$\overline{P_m} - P_f = \frac{\mu\, B_o\, q_o\, {L_f}^2}{12\, k_m\, V_m} \tag{4.23}$$

4.3.2.4 Average matrix pressure based on Pseudo-steady state flow

Expressing P_f as a function of time,

$$c_t = -\frac{1}{\phi_m V_m}\frac{\Delta V_o}{\Delta P_m} \tag{4.24}$$

$$C_t\, V_m\, dP_m = -dV_m \tag{4.25}$$

Here,

$$\Delta P_m = P_i - \overline{P_m} \quad and \quad \Delta V_o = B_o\, q_o\, t \tag{4.26}$$

$$\phi_m V_m = \phi_m\, L_f\, h\, 2y_e \tag{4.27}$$

Substituting Eq. 4.26 and 4.27 in Eq. 4.24,

$$\overline{P_m} - P_i = \frac{B_o\, q_o\, t}{L_f h\, 2y_e\, \phi_m\, c_t} \tag{4.28}$$

4.3.2.5 Final Solution

Replacing $\overline{P_m}$ from Eq. 4.23

$$P_i - P_f = \frac{B_o q_o\, t}{L_f\, h\, 2y_e\, \phi_m\, c_t} + \frac{\mu\, B_o\, q_o\, {L_f}^2}{12\, k_m\, V_m} \tag{4.29}$$

We know $N_p = q_o\, t$ (4.30)

Replacing Eq. 4.30 in Eq. 4.29 and dividing by q_o we obtain

$$\frac{P_i - P_f}{q_o} = \frac{B_o \quad N_p}{L_f\, h\, 2y_e\, \phi_m\, c_t\, q_o} + \frac{\mu\, B_o\, q_o\, {L_f}^2}{12\, k_m\, V_m} \tag{4.31}$$

Replacing $\frac{N_p}{q_o} = \bar{t}$ (4.32)

$$\frac{Pi - P_{wf}}{q_o} = \frac{B_o\, \bar{t}}{L_f\, h\, 2y_e\, \phi_m\, c_t} + \frac{\mu\, B_o\, {L_f}^2}{12\, k_m\, V_m} \tag{4.33}$$

$\bar{t}$ is the material balance time (MBT)

N_p is the cumulative oil production

Q_o is the daily oil rate

Blasingame and Lee (1986) introduced the original material balance approach for boundary-dominated flow (i.e. pseudo steady state flow), which is later modified by Placio and Blasingame (1993) for any instantaneous production time, flow regime or production scenario.

When the boundary effects are observed after the transient flow regime, we assume $P_f = P_{wf,}$ this means that the pressure drop in the fracture is negligible.

$$\frac{Pi - P_{wf}}{q_o} = \frac{B_o\,\bar{t}}{L_f\,h\,2y_e\,\phi_m\,c_t} + \frac{\mu\,B_o\,{L_f}^2}{12\,k_m\,V_m} \tag{4.33}$$

Eq. 4.33 is developed for one producing fracture; to incorporate the effect of multiple numbers of fractures we multiply q_o and V_m by number of fractures N_f to obtain total flow rate Q_o and total reservoir volume.

$$\frac{Pi - P_{wf}}{Q_o} = \frac{B_o\,\bar{t}}{A_{cw}\,y_e\,\phi_m\,c_t} + \frac{\mu\,B_o\,{L_f}^2}{12\,k_m\,N_f\,V_m} \tag{4.34}$$

$\frac{Pi-P_{wf}}{q_o}$ is defined in the petroleum literature as Rate-Normalized Pressure (RNP).

To analyze the boundary dominated flow we plot RNP versus MBT.

$$\frac{Pi - P_{wf}}{Q_o} = m_{ss}\,\bar{t} + b_{ss} \tag{4.35}$$

Here m_{ss} and b_{ss} are the slope and intercept of the line on the plot of RNP versus MBT given by:

$$m_{ss} = \frac{5.615\,B_o}{A_{cw}\,y_e\,\phi_m\,c_t} \tag{4.36}$$

By replacing $SRV = A_{cw} \times y_e \times \varphi_m$ in Eq. 4.36 we obtain

$$m_{ss} = \frac{5.615\,B_o}{SRV\,c_t} \tag{4.37}$$

The intercept is given by

$$b_{ss} = \frac{\mu \, B_o \, L_f^{\,2}}{12 \, k_m \, N_f \, V_m} \tag{4.38}$$

Replacing V_m from Eq. 4.11 and converting to field units

$$b_{ss} = \frac{36.96 \, \mu \, B_o \, L_f}{k_m \, N_f \, y_e \, h} \tag{4.39}$$

Using m_{ss} we calculate the stimulated reservoir volume SRV. Comparing with SRV calculated from transient region, we identify whether the pressure interference has occurred not. If the value of SRV obtained from matrix analysis is very high as compared to the value obtained from analysis of the boundary-dominated flow, we can say that the reservoir has not been depleted completely. Another explanation is that the fracture half-length y_e is over estimated. Similarly we can identify if the number of fracture is optimum for efficient reservoir depletion or not.

By analyzing the intercept of the line (b_{ss}) we can estimate the minimum permeability of the reservoir (Song and Economides 2011). For homogenous reservoirs, the value calculated from this analysis should be approximately equal to the permeability obtained by well testing.

CHAPTER V

PRODUCTION DATA ANALYSIS OF GAS RESERVOIRS IN BARNET SHALE

5.1 INTRODUCTION

Shale gas reservoirs play a major role in the United States natural gas supply. The unconventional shale gas reservoirs that are the focus of this study are self-sourcing reservoirs. The shale acts as both the source rock and reservoir. In shales, natural fractures provide permeability and the matrix provides storage of most of the gas. Shale permeability can be as low as 10^{-9} md.

The Gas Technology Institute estimates that organic shale reservoirs in United States contain up to 780 tcf of gas. The Barnet Shale in the Fort Worth Basin is by far most active shale gas play in the United States. Horizontal wells producing gas in the Barnet Shale are typically multi-stage hydraulic fractured.

Mayerhofer et al (2006) present a model for hydraulically fractured shale gas reservoirs. Their model represents the hydraulic fracture as interconnected network of fractures. Their paper indicates that drainage does not occur far beyond the stimulated region because of low matrix permeability.

Linear flow is the dominant flow regime for fractured horizontal wells in tight formations for most of their production lives (Medeiros et al (2008). Many other authors (Bello 2009, Bello and Wattenbarger 2008, 2009, Al-Ahmadi et al 2010) also observed that the wells in tight formations (such as Barnett Shale) are controlled by transient linear flow.

A negative half-slope on the log-log plot characterizes this behavior. However, a bi-linear flow is also observed just before the linear flow in some shale gas reservoirs. A negative quarter-slope on the log-log plot characterizes this behavior. This bi-linear flow is due to the simultaneous depletion of two connected media. The two media could be micro-fractures and matrix or micro-fractures and macro-fractures.

Shale gas wells have been modeled using linear dual-porosity models. Some of the horizontal wells drilled in shale gas reservoirs are hydraulically fractured. According to Gate et al (2007), propagation of these hydraulic fractures re-activate the pre-existing natural fractures resulting in the two perpendicular fractures systems with different properties. Therefore, dual porosity models (which assume homogeneous matrix properties) are not sufficient to characterize these reservoirs, as the matrix permeability will be enhanced by reactivated natural fractures. A triple porosity model is thus required to model horizontal shale gas wells containing reactivated (or pre-existing) natural fractures.

This chapter deals with analysis of Region 4 and Region 5 in detail. A preliminary procedure is also presented for analyzing field data.

5.2 Procedure For Production Data Analysis for Tight Gas Wells

In this section we present the procedure to analyze the production data of tight gas reservoir using triple porosity equations developed in Chapter III of this dissertation. After obtaining the field data, we identify different flow regions by constructing a specialized plot of flow rate versus material balance time. The procedure for analyzing Region 4 and Region 5 as define in Chapter III is presented below.

5.2.1 Region 4 (Bilinear Flow in Micro-fractures and Matrix)

Region 4 can be analyzed by following the steps presented below:

1. Identify the transient flow region indicated by quarter slope on the log-log plot of flow rate against material balance time.
2. Plot Rate Normalized pseudo-pressure (RNP) $\frac{m(P_i)-m(P_{wf})}{Q_g}$ versus $\sqrt[4]{\bar{t}}$

3. Use the slope of the line (m_4) to calculate either k_f or L_f if one of them is known, or if k_f and L_f are not known we can calculate the ratio of $\frac{k_f}{L_f}$ using

$$\frac{L_f}{L_F}\sqrt{k_f}A_{cm} = \frac{2004T}{\sqrt[4]{k_m(\text{Ø}\mu c_t)_m}}\frac{1}{m_4}$$

5.2.2 Region 5 (Rate Transient Flow from Matrix)

Region 5 can be analyzed by following the steps presented below:

1. Identify the transient flow region indicated by a half slope on the log-log plot of flow rate against material balance time.
2. Plot Rate Normalized Pressure (RNP) $\frac{m(P_i)-m(P_{wf})}{Q_g}$ versus $\sqrt{t}$ for gas wells.
3. Use the slope of the line (m_5) to calculate area of interface between matrix and hydraulic fractures A_{cm} from

$$\sqrt{k_m}A_{cm} = \frac{2182T}{\sqrt{(\text{Ø}\mu c_t)_m}}\frac{1}{m_5} \qquad (5.2)$$

4. The number of micro fractures (n_{fye}) can be calculated using

$$n_{fye} = \frac{A_{cm}}{2\,A_{cw}} \qquad (5.3)$$

5.3 APPLICATION OF ANALYSIS PROCEDURE TO PRODUCTION DATA

In this section we use the developed triple porosity model to analyze the field data of two wells from Barnett Shale i.e. well 314 and well 73. Gas rate history of these well is shown in **Fig. 5.1** (Al-Ahmadi 2010).

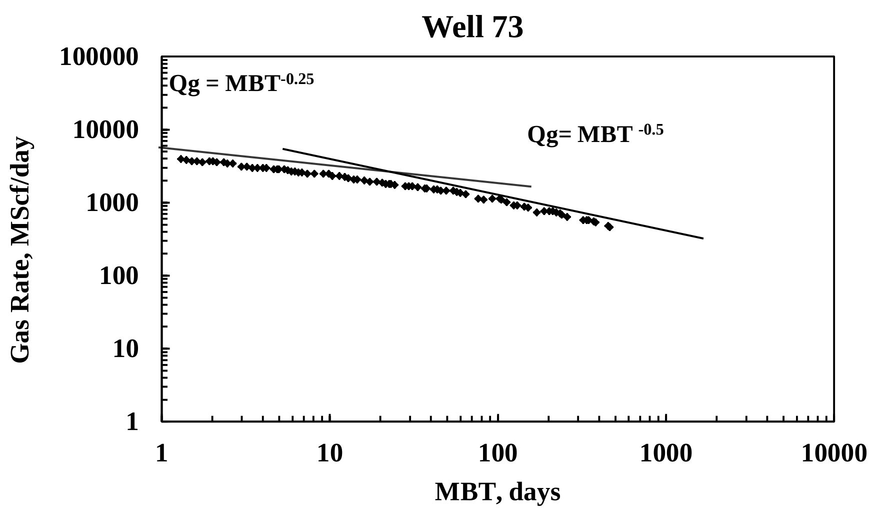

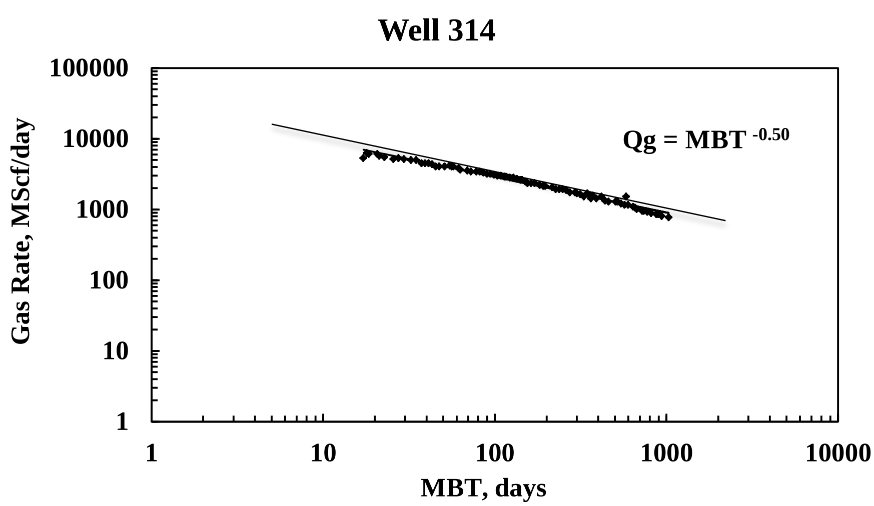

Fig. 5.1 – Log-log plot of gas rate versus time for two horizontal shale gas wells. Well 73 exhibits bi-linear flow between micro fracture and matrix followed by matrix linear flow as it gives negative quarter-slope for some time and then negative half-slope. Well 314 shows negative half-slope for almost two log cycles and indicates matrix linear flow.

5.3.1 Production Data Analysis of Well 73

Table 5.1 summarizes the petro-physical and completion data of Well 73.

Table 5.1 Reservoir and fluid properties obtained from well tests of Well 73

Reservoir Type	Homogeneous	Permeability – Horizontal **(k)**	1.50E-04 md
Dominant Flow	Gas	Reservoir thickness **(h)**	300 ft.
Multiphase flow in reservoir	No	Matrix Porosity **(ϕ_m)**	0.06
Reservoir Pseudo pressure **$m(P_i)$**	5.97E+08 psi^2/cp	Fracture Spacing **(L)**	79 ft.
Flowing BHP **$m(P_{wf})$**	2.03E+07 psi^2/cp	Gas viscosity **(μ_{gi})**	0.0201 cp
Number of stages of fractures	18	Temperature (**T**)	610 ^0R
Length of horizontal well **(X_e)**	1420 ft.	Total Compressibility **(c_t)**	3.00E-04 psi^{-1}

5.3.1.1 Analysis of bilinear transient region

We consider the production data of well 73 till the point it exhibits a negative quarter slope as shown in Fig.5.2. In Fig. 5.3 we plot RNP versus fourth root of time.

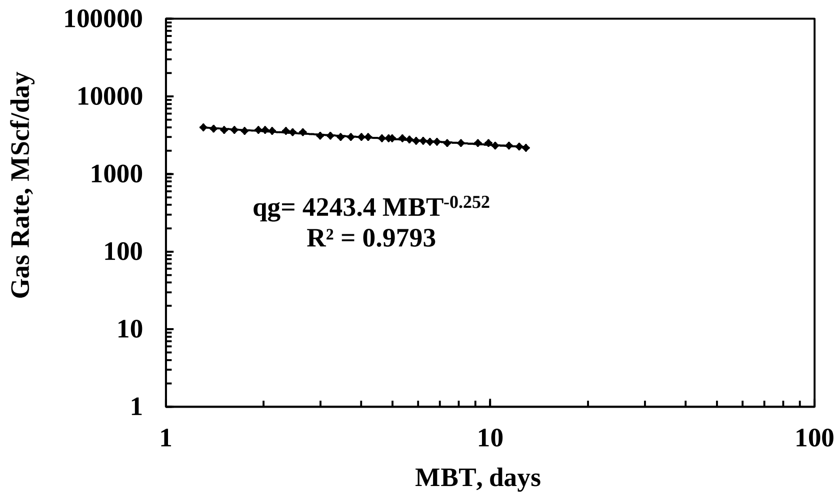

Fig. 5.2 – Log-log plot of gas rate versus MBT that shows a negative quarter slope.

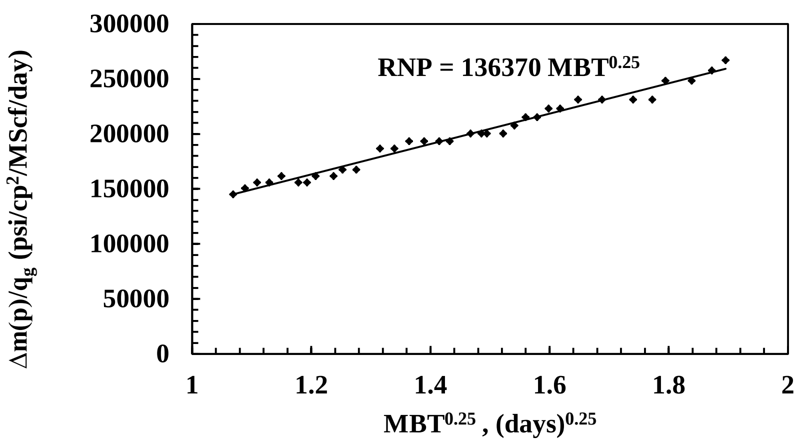

Fig. 5.3 – Plot of fourth root MBT versus RNP that gives slopes equal to 136370 psi/cp^2/Mscf/day/day$^{0.25}$

Now we use Eq.5.1 for analysis of Region 4 to obtain the ratio $\frac{k_f}{L_f}$. Slope m_4 is found to be 136370 psi/cp^2/Mscf/day/day$^{0.25}$. If we assume stimulated fracture half-length $y_e = 150$ ft then $\frac{k_f}{L_f}$ is calculated by,

$$\sqrt{\sigma_F} y_e \sqrt{\frac{k_f}{L_f}} A_{cw} = \frac{2004T}{\sqrt[4]{k_m(\emptyset\mu c_t)_m}} \frac{1}{m_4}$$

$$\sqrt{\frac{12}{79^2}} \times 150 \times \sqrt{\frac{k_f}{L_f}} \times 85200 = \frac{2004x610}{\sqrt[4]{(1.5x10^{-4}x3.62x10^{-7})}} \times \frac{1}{136370}$$

$$\frac{k_f}{L_f} = 0.000626 \ {}^{md}/_{ft}$$

5.3.1.2 Analysis of Linear Transient Region (Matrix)

We consider the part of production data that shows linear flow i.e. Region 5. We plot RNP versus square root of MBT as shown in Fig. 5.4. In Fig. 5.5 we plot RNP versus fourth root of time. Reservoir data and other parameters used are same as in Table 5.1.

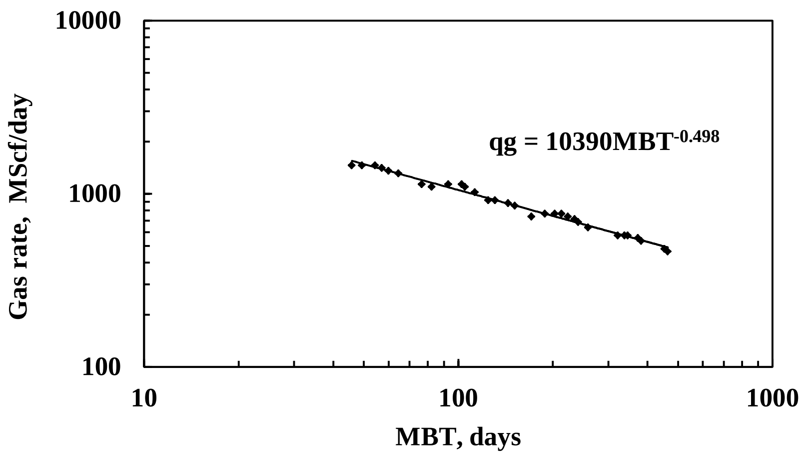

Fig. 5.4 – Log-log plot of gas rate versus MBT shows a negative half slope.

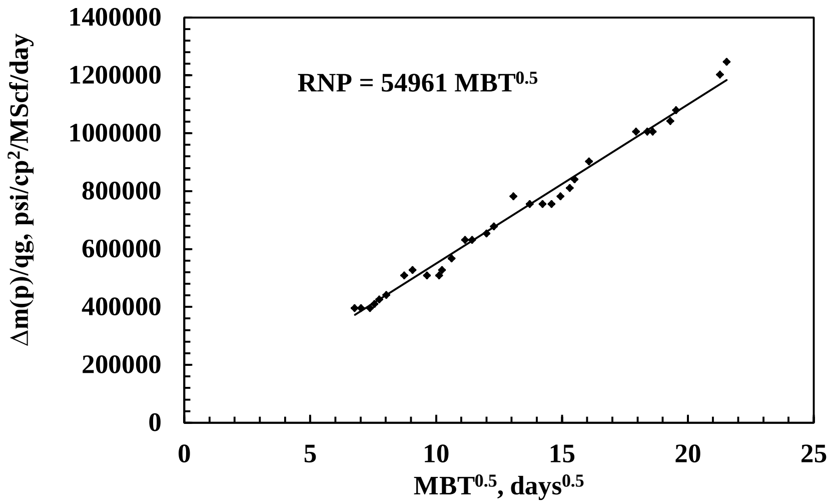

Fig. 5.5 – Plot of square root MBT versus RNP that gives slopes equal to 54961 psi/cp^2/Mscf/day/day$^{0.5}$

From Fig-5.5 slope is found to be 54961 psi^2/cp/MScf/day/day$^{0.5}$. We use Eq. 5.2 to calculate the drainage area A_{cm}.

$$\sqrt{k_m}A_{cm} = \frac{1262T}{\sqrt{(\O\mu c_t)_m}}\frac{1}{m_5}$$

Replacing the corresponding values,

$$\mathrm{A_{cm}} = \frac{(1262)(610)}{\sqrt{(1.5\mathrm{x}10^{-7})(3.62\mathrm{x}10^{-7})}} \times \frac{1}{54961} = 1{,}900{,}000\ \mathrm{ft}^2$$

Now we calculate the number of micro-fractures $\mathrm{n_{f_{y_e}}}$ using Eq. 5.3,

$$\mathrm{A_{cm}} = \left(2\mathrm{n_{f_{y_e}}}\mathrm{A_{cw}}\right)$$

$$\mathrm{n_{f_{y_e}}} = \frac{\mathrm{A_{cm}}}{2\mathrm{A_{cw}}} = \frac{1900000}{2 \times 852000} = 1$$

5.3.2 Regression Results for Well 73

Al-Ahmadi (2010) used Least Absolute Value (LAV) regression analysis technique to determine the unknown parameters in his transfer function. He assumed the values of the macro-fracture and micro-fracture storativity and porosity. The assumed values are shown in Table 5.2.

Table 5.2 Values of Assumed Parameters for Regression for Well 73

Parameter	**Assumed Values**
Φ_F	0.2
ω_F	0.1
Φ_f	0.01
ω_f	0.01

The results obtained after regression are shown in Table 5.3 (Al-Ahmadi 2010).

Table 5.3 Regression results for Well 73 (Assuming no adsorption)

Parameter	**LAV Results**
k_F , mD	3.7
k_f, mD	0.1
L_f , ft	23
y_e , ft	185

5.3.2.1 Comparison of Results

The results obtained from analytical equations vary significantly from results obtained from regression analysis. The production data doesn't usually contain flow data from early time scales (fluid production from macro fractures and micro-fractures). If the fracture properties are assumed, the regression results will be affected. The regression results depend on the initial assumed value and can vary if the initial guess made is not close.

5.3.3 Production Data Analysis of Well 314

The production data for this well only exhibits linear flow that reflects the matrix depletion. Reservoir data is summarized in Table 5.4. The production data plot is shown in Fig. 5.6.

Table 5.4 Reservoir and fluid properties obtained from well tests of Well 314

Reservoir Type	Homogeneous	Permeability – Horizontal **(k)**	1.50E-04 md
Dominant Flow	Gas	Reservoir thickness **(h)**	300 ft.
Multiphase flow in reservoir	No	Matrix Porosity (**φ**)	0.06
Reservoir Pseudo pressure **$m(P_i)$**	5.97E+08 psi^2/cp	Fracture Spacing (**L**)	106 ft.
Flowing BHP **$m(P_{wf})$**	2.03E+07 psi^2/cp	Gas viscosity (**μ_{gi}**)	0.0201 cp
Number of stages of fractures	28	Temperature (**T**)	610 ^{0}R
Length of horizontal well (**X_e**)	2968 ft.	Total Compressibility (**c_t**)	3.00E-04 psi^{-1}

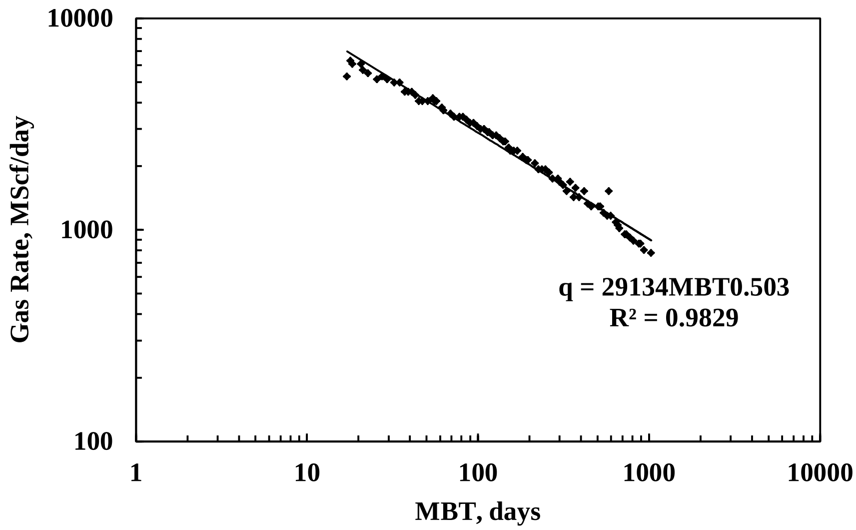

Fig. 5.6 – Log-log plot of gas rate versus MBT shows a negative half slope.

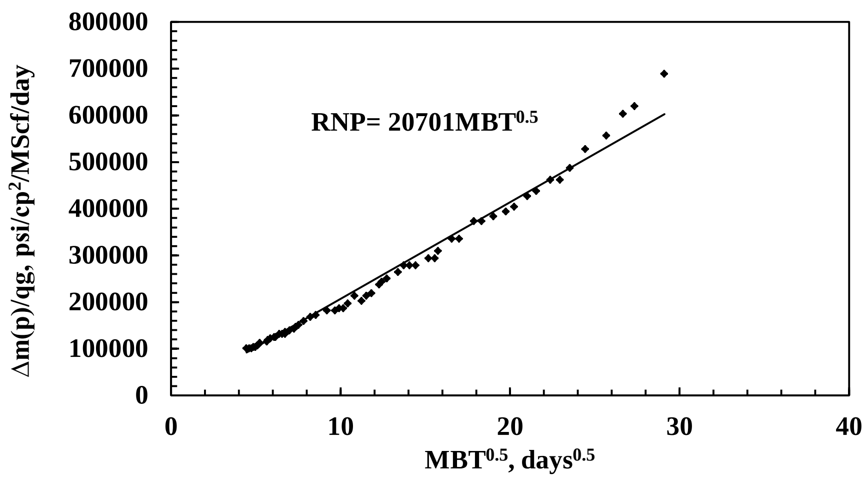

Fig. 5.7 – Plot of square root MBT versus RNP that gives slopes equal to 20701 psi/cp^2/Mscf/day/day$^{0.5}$

Figure 5.7 shows the square root time plot slope is equal to 20701 psi^2/cp/MScf/day/day$^{0.5}$. Using Eq. 5.2 to calculate $A_{cm.}$

$$\sqrt{k_m}A_{cm} = \frac{1262T}{\sqrt{(\O\mu c_t\ )_m}}\frac{1}{m_5}$$

Replacing the corresponding values in Eq. 5.2

$$A_{cm} = \frac{(1262)(610)}{\sqrt{(1.5x10^{-4})(3.62x10^{-7}\ )}} \times \frac{1}{20701} = 5{,}050{,}000\ ft^2$$

Using Eq. 5.3 to calculate the number of micro-fractures.

$$n_{f_{y_e}} = \frac{A_{cm}}{2A_{cw}} = \frac{5050000}{2\ \times\ 1780800} \cong 1$$

5.3.4 Regression Results for Well 314

The assumed values are for regression is shown in Table 5.5.

Table 5.5 Values of Assumed Parameters for Regression for Well 314

Parameter	Assumed Values
Φ_F	0.2
ω_F	0.1
Φ_f	0.01
ω_f	0.01

The results obtained after regression are shown in Table 5.6.

Table 5.6 Regression results for Well 314 (Assuming no adsorption)	
Parameter	**LAV Results**
k_F , mD	10.9
k_f , mD	0.26
L_f , ft	24
y_e , ft	205

5.3.4.1 Comparison of Results

The results for Well 314 obtained from regression also vary from our analysis. The results can be interpreted similarly as Well 73.

5.3.5 Summary and Discussion of Results

The analysis results of both wells show that the number of micro fracture(s) is 1, which means that only one connected micro-fracture is enough to create the required interface for the matrix depletion (In the absence of fluid transfer between matrix and hydraulic fracture). We consider the following two interpretations.

- A dual porosity model is more suitable to characterize this reservoir and the early region (bilinear flow) observed during production is because of simultaneous depletion of hydraulic fractures and matrix.
- If the micro fractures are present they are not connected. A higher number of smaller fractures are still possible for this case.

CHAPTER VI

PRODUCTION DATA ANALYSIS OF TIGHT OIL RESERVOIRS

6.1 INTRODUCTION

Recent advances in horizontal drilling and multi-stage hydraulic fracturing have led to the successful exploitation of tight oil and shale gas reservoirs.

Clarkson and Pedersen (2011) proposed the term "Unconventional Light Oil" (ULO) and proposed further categories of ULO on the basis of play types and matrix permeability. Reservoir properties that could distinguish ULO plays from conventional light oil plays also include low matrix permeability (<0.1 md). A classification for the ULO plays in Western Canada is as follows:

1. Halo Oil **–** High matrix permeability (e.g. Cardium and Viking Pools of Alberta)
2. Tight Oil **–** Low matrix permeability (e.g. Saskatchewan Bakken Formation)
3. Shale Oil **–** Very low matrix permeability (e.g. Duvernay and Muskwa Formations)

This chapter deals with the analysis of tight oil wells from Cardium and Bakken formations. The production data of tight oil wells exhibit linear transient behavior that is analyzed using the dual porosity models. The linear transient flow from matrix depletion is analyzed using dual porosity model presented by Bello (2009). The boundary dominated flow (that occurs under pseudosteady state flow conditions) is analyzed by the model developed in Chapter IV of this work.

6.1.1 Pembina Cardium (Halo Oil)

Cardium Formation is the largest conventional oil reserves in the Western Canada Sedimentary Basin. The oil production initiated in the early 1950s, and only approximately 20% of the reserve is recovered. The Cardium Formation (deposited in the Late Cretaceous, approximately 88 million years ago) consists of interbedded sandstone and shale, and some local conglomerate, spread over much of western Alberta. Over the past fifty years, conglomerates and porous sandstones have been targeted for conventional production of oil, mainly from the Pembina Field. The Cardium Formation in Alberta is estimated to have contained 1,678 million m^3 (10.6 billion barrels) of oil originally in place, 1,490 million m^3 (9.4 billion barrels) of which was in the Pembina Field. Since its discovery in the 1950s, 234 million m^3 (1.5 billion barrels) of Cardium oil has been produced. Production of oil in the Cardium Formation rebounded in 2009, when horizontal drilling and multi-stage fracturing technology increased the oil recovery factor.

6.1.2 Saskatchewan Bakken (Tight Oil)

The Bakken Formation in Saskatchewan and Manitoba is a part of a relatively thin accumulation of siltstone and sandstone sandwiched between organic-rich shales extending over much of western Canada. It was deposited as the Devonian Period transitioned into the Mississippian Period, approximately 360 million years ago. The Bakken tight oil play is about 25 meters thick and consists of lower organic-rich shale, a middle siltstone and sandstone unit, and overlying organic-rich shale.

So far, companies have publicly reported 36 million m^3 (225 million barrels) of proved and probable reserves from the Bakken. No reserves from the Exshaw have been publicly reported. Where the Bakken extends into North Dakota and Montana, the United States Geological Survey estimates that there are 580 million m^3 (3.65 billion barrels) of recoverable oil. The areal extent of oil-prone Bakken in the United States is far more extensive than in Saskatchewan.

6.2 Procedure for Production Data Analysis of Tight Oil Reservoirs

In this section we present a procedure for analyzing the production data of tight oil reservoirs using the dual porosity equations. The boundary dominated flow (pseudosteady state flow) is analyzed using the equations developed in Chapter IV. After obtaining the field data, we identify different flow regions by constructing a specialized plot of flow rates versus material balance time. Analysis procedure of matrix flow and boundary dominated flow is discussed below.

6.2.1 Analysis of Transient Matrix Depletion (Dual porosity systems)

Transient linear flow from matrix is analyzed by the following steps:

1. Identify the transient flow region by half slope on the log-log plot of flow rate against material balance time
2. Plot Rate Normalized Pressure (RNP) $\frac{P_i - P_{wf}}{Q_o}$ against material balance time $\sqrt{\bar{t}}$ for oil wells
3. Use slope of the line (m) in the analysis equation presented by Bello (2009) for the dual porosity systems to calculate area of interface between matrix and hydraulic fractures A_{cm}:

   $$\sqrt{k_m}A_{cm} = \frac{125.11\, B\, \mu}{\sqrt{(\emptyset \mu c_t)_m}} \frac{1}{m}$$

4. Calculate the effective fracture half length y_e by using following equation

   $$y_e = \frac{A_{cm}\, L_F}{A_{cw}}$$

   Where,

   L_F is the spacing between hydraulic fractures

6.2.2 Analysis of boundary dominated flow (PSS flow)

Boundary dominated flow can be analyzed by the following steps:

1. Construct a log-log plot between rate-normalized pressure (RNP) and material balance time (MBT) for the complete production data.
2. The region for the pseudo steady flow is recognized by a constant slope of one on a log-log plot of flow rate versus MBT.
3. Plot RNP versus MBT of data points of pseudo steady state flow region on a linear scale.
4. Record the line slope, m_{ss}, and the line intercept, b_{ss}
5. Calculate the stimulated reservoir volume SRV by substituting m_{ss} in

   $$m_{ss} = \frac{5.615\ B_o}{SRV\ c_t}$$

6. Calculate the minimum permeability of the reservoir by substituting b_{ss} in

   $$b_{ss} = \frac{36.96\ \mu\ B_o\ L_f}{k_m\ N_f\ y_e\ h}$$

6.3 PRODUCTION DATA ANALYSIS OF CARDIUM WELLS

In this section, we analyze the production data of tight oil wells drilled in Cardium formation.

6.3.1 Observing behavior of Cardium Wells

We analyze production data from several oil wells drilled in Cardium formation to identify different flow regimes. Figure 6.1 shows log-log plot of cumulative oil production versus time. The advantage of such plots is the insensitivity to shut-ins and fluctuations in production rate. The slope of this plot may indicate the dominant flow regimes (El Banbi 1998).

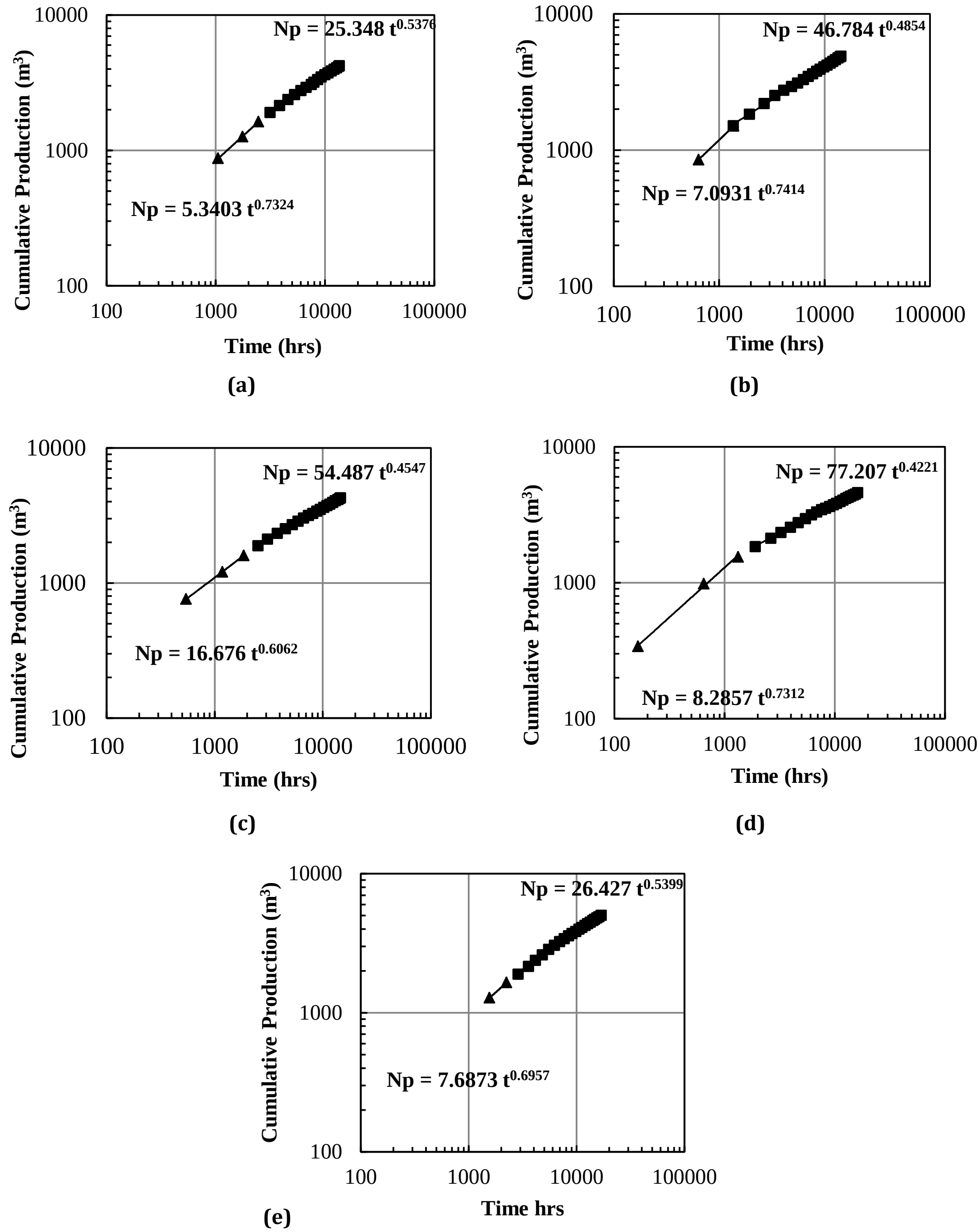

Fig. 6.1 – Plots of cumulative oil production versus time for five fractured horizontal wells completed in Cardium formation. The log-log plots show a slope of 0.6 - 0.75 for early time scales and a slope of approximately 0.5 for late time scales. The length of horizontal wells and number of stages of hydraulic fractures are different in these wells. The consistent behavior of cumulative plots shows that the flow regime is relatively similar for all the wells.

Da Prat el al (1981) recognized that for linear flow regime, dimensionless cumulative production Q_D versus dimensionless time on a log-log plot gives a slope of 0.5. They observed this linear flow behavior for transient dual porosity case. Therefore it can be interpreted from the second part of these plots that the dominant flow regime in Cardium wells is also linear transient. The first region can be interpreted as bi-linear flow. Therefore, the analysis equation developed for linear flow for slightly compressible fluid can be applied here.

6.3.2 Example Application for Characterizing a Fractured Well in Cardium Formation

We select a tight oil well in a Pembina field. The well is hydraulically fractured (18 multi stages) and has been producing for nearly 2 years. The fluctuation in production rate were caused by shut-ins. Unfortunately, complete information about those shut-in periods is not available. **Table 6.1** presents the available fluid and reservoir properties.

Table 6.1 Reservoir and fluid properties of Well in Cardium Formation

Reservoir Type	Homogeneous	Permeability–Horizontal **(k_{hor})**	0.640 mD
Dominant Flow	Oil Phase	Permeability–Vertical **(k_{ver})**	9.03×10^{-4} mD
Multiphase flow in reservoir	No	Reservoir thickness **(h)**	7 m
Reservoir Pressure **(P_i)**	15,575 KPaa	Matrix Porosity **(ϕ_m)**	0.120
Flowing BHP **(P_{wf})**	7,413 KPaa	Oil Formation Volume factor **(B_o)**	1.221 Rm^3 / m^3
Number of stages of fractures	18	Oil Viscosity **(μ_o)**	1.13 cp
Length of horizontal well **(X_e)**	1370 m	Total Compressibility **(c_t)** (Assumed)	1.54×10^{-4} psi^{-1}

We assume that the oil flows directly into the hydraulic fractures since the vertical permeability is very low as compared to the horizontal permeability. **Figure 6.2** shows the daily oil rate versus time on a log-log plot. The data indicates that the production rates are variable and therefore it is difficult to distinguish any flow regimes from this plot.

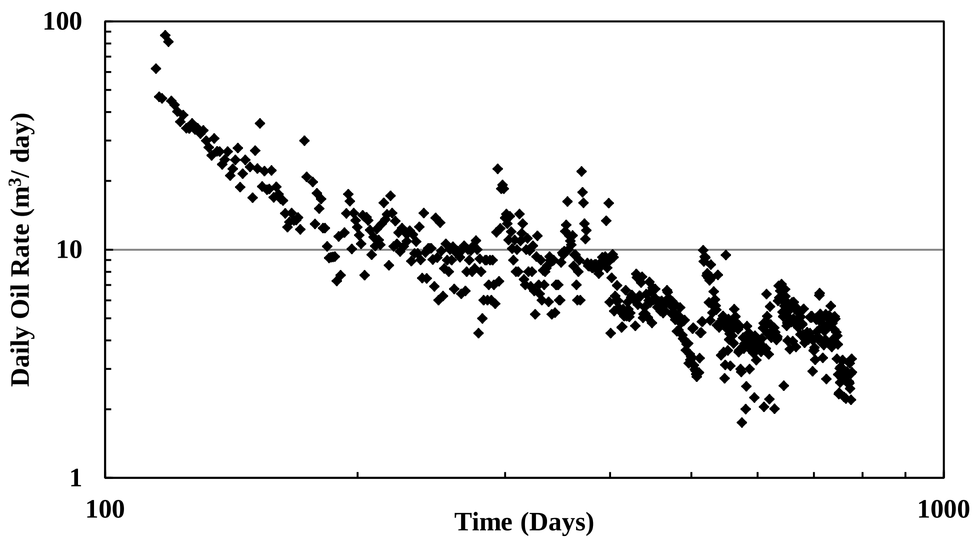

Fig. 6.2 – Log-log plot of daily oil rate versus time for a Well in Cardium Formation

In order to identify different flow regimes, we plot the production rate versus material balance time. **Figure 6.3** shows the log-log plot of oil rate versus material balance time for the same well in which three distinctive flow regions can easily be identified. Region 1 shows of negative half-slope during maximum life of production and Region 2 shows a negative slope of one.

We assume that Region 1 (transient matrix flow) represents linear transient flow from the matrix into the hydraulic fractures. This assumption is supported by low vertical permeability in Cardium formation. We apply the dual porosity model of Bello (2009) to analyze this region. Furthermore we assume that Region

2 (boundary dominated flow) represents PSS matrix depletion when pressure interference has occurred between two adjacent fractures. We use the PSS model developed in this work to analyze this region.

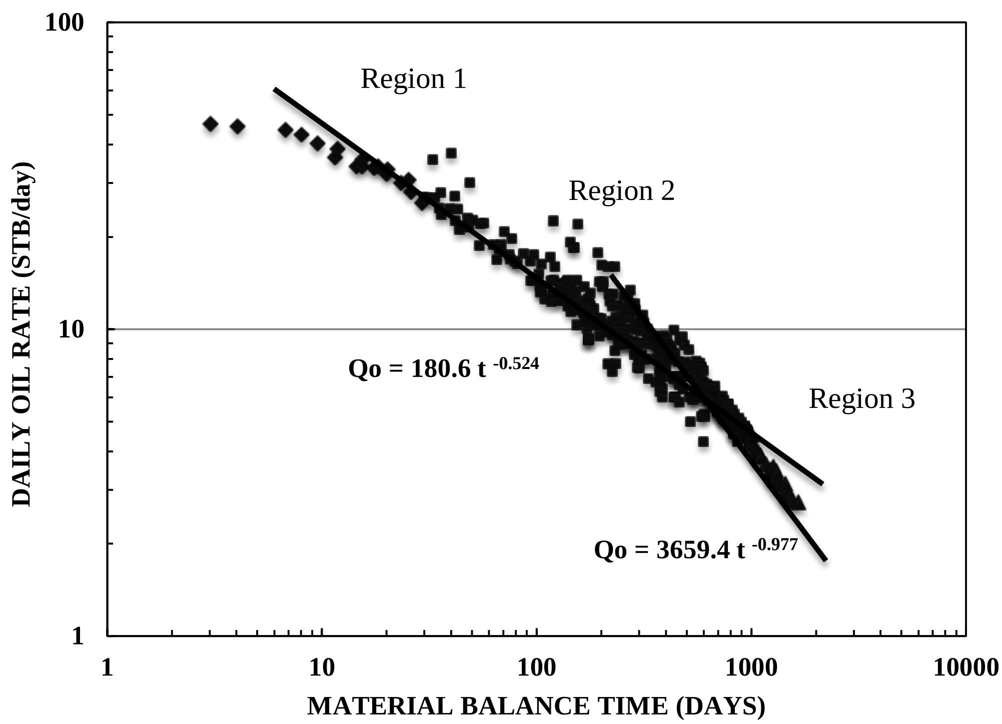

Fig. 6.3 – Log-log plot of daily oil rate versus calculated material balance time of the well in Cardium Formation.

Region 1 is not analyzed, as the production data of this region is very limited. This region can also be the representative of well bore storage.

6.3.2.1 Analysis of Linear Transient Region

In **Fig. 6.4** we plot RNP versus MBT.

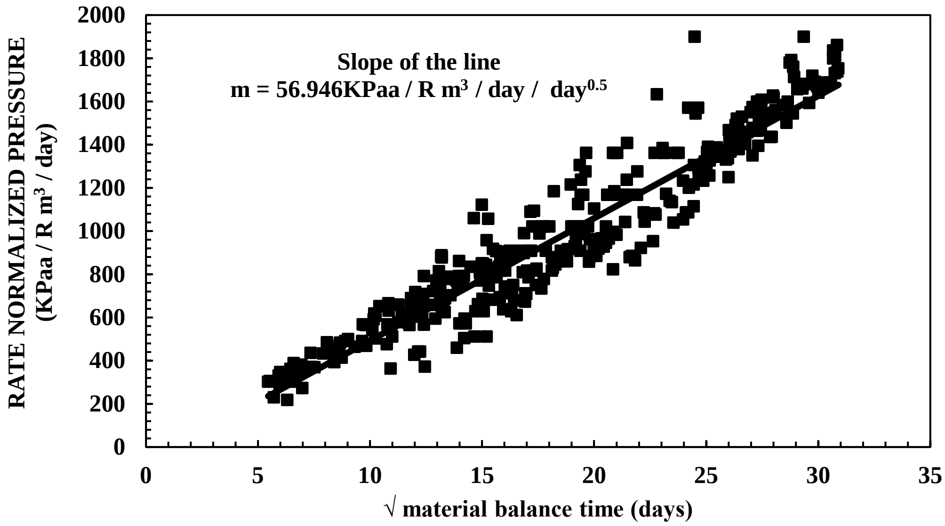

Fig. 6.4 – Specialized plot of Rate Normalized Pressure versus square root of Material Balance Time for analyzing flow from matrix to fracture

We substitute the value of m, determined in Fig. 6.4, in the analysis equation of dual porosity model and calculate the fracture-matrix interface area A_{cm}:

$$\sqrt{k_m}A_{cm} = \frac{125.11\ B\ \mu}{\sqrt{(\emptyset\mu c_t)_m}}\frac{1}{m}$$

Slope of the line m = 56.946 KPaa / R m^3 / day / day$^{0.5}$ or 1.313 psi / res bbl / day / day$^{0.5}$

$$A_{cm} = \frac{125.11\ \times 1.221\ \times\ 1.13}{\sqrt{0.640}\sqrt{(0.12\ \times\ 1.13\ \times\ 1.52\ \times\ 10^{-4})}}\frac{1}{1.313}$$

$$A_{cm} = 36{,}197.60\ \text{ft}^2$$

Using Eq. 3.11 to determine A_{cw}

$$A_{cw} = 2\ \times\ X_e\ \times h$$

$A_{cw} = 2 \times 1370 \times 7 \times 3.28^2 = 206{,}346.11$ ft^2

Stimulated fracture half-length y_e is calculated using $y_e = \frac{A_{cm}}{A_{cw}} \times L_f$

$$y_e = \frac{36{,}197.60 \times 76 \times 3.28}{206{,}346.11}$$

$y_e = 43.73$ ft or 13.33 m

The stimulated reservoir volume ($SRV = 2 \times X_e \times h \times \phi_m \times y_e$) is calculated to be 1,082,800 ft^3 or 30,685.05 m^3.

6.3.2.2 Analysis Of Boundary Dominated Flow Region

In **Fig. 14,** we plot RNP versus MBT

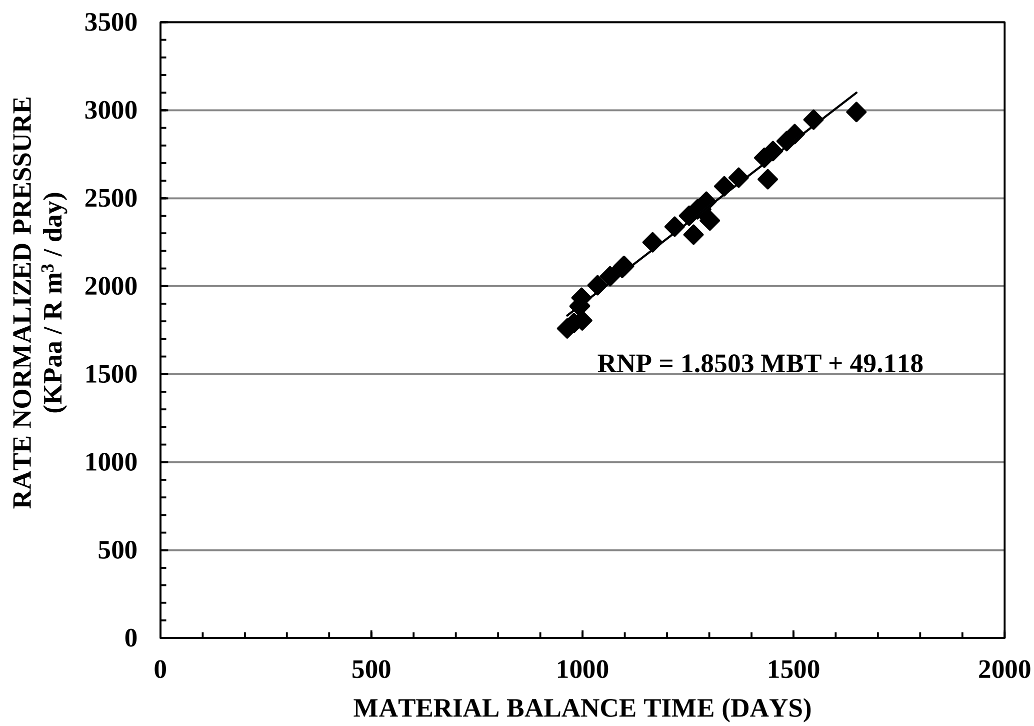

Fig. 6.5 – Specialized plot of RNP versus MBT for analyzing boundary dominated flow of the well completed in Cardium Formation.

Slope of the line m_{ss} = 1.8503 KPaa / R m^3 / day / day or 0.0427 psi / STB / day / day

and b_{ss} = 49.118 KPaa / Rm^3 / day or 1.134 psi / STB / day

Using Eq. 6.2

$$m_{ss} = \frac{5.615\, B_o}{A_{cw}\, y_e\, \phi_m\, c_t}$$

We also know that Stimulated Reservoir Volume $(SRV) = A_{cw}\, y_e\, \phi_m$.

Therefore,

$$SRV = 5.615 \frac{B_o}{c_t} \frac{1}{m_{ss}}$$

$$\mathrm{SRV} = 5.615 \frac{1.221}{1.52 \times 10^{-4}} \frac{1}{0.0427}$$

$$\mathrm{SRV} = 1{,}056{,}316.2\ \mathrm{ft}^3 \text{ or } \mathrm{SRV} = 29{,}934.53\ \mathrm{m}^3$$

Now, we use the intercept equation to determine the matrix permeability:

$$b_{ss} = \frac{36.96\, \mu\, B_o\, L_f}{k_m\, N_f\, y_e\, h}$$

$$k_m = \frac{36.96\, \mu\, B_o\, L_f}{b_{ss}\, N_f\, y_e\, h}$$

$$k_m = \frac{36.96 \times 1.13 \times 1.221 \times 76 \times 3.28}{1.134 \times 18 \times 43.73 \times 7 \times 3.28}$$

$$k_m = \ 0.620\ \mathrm{mD}$$

6.3.3 Summary of Results

The analysis results are summarized in Table 6.2

Table 6.2 Unknown reservoir parameters obtained by analyzing matrix transient region and boundary dominated region of production data of the well completed in Cardium Formation

PARAMETER	VALUE
Slope of line for matrix region **m**	1.313 psi / res bbl / day / $day^{0.5}$
Slope of line for PSS region $\mathbf{m_{ss}}$	0.0427 psi / STB / day / day
Intercept of the line b_{ss} (PSS region)	1.134 psi / STB / day
Permeability - k	0.620 mDarcy (From PSS Analysis)
	0.640 mDarcy (Well Tests)
Total Reservoir Area - $\mathbf{A_{cw}}$	19180 sq.m or 206,346.112 sq.ft
Drainage Interface - $\mathbf{A_{cm}}$	3364.5 sq.m or 36,197 sq.ft
Effective fracture half length - $\mathbf{y_e}$	13.33 m or 43.72 ft.
Stimulated Reservoir Volume **SRV**	30,685 m^3 (Matrix Analysis)
	29,934 m^3 (Pseudo steady state Analysis)

The value of SRV obtained by analyzing linear transient region is similar to that obtained by analyzing the PSS region. Furthermore, the value of permeability obtained by well testing and that obtained by our PSS analysis are very close to each other (See Table 6.2).

6.4 Example Application for Characterizing a Fractured Well in Bakken Formation

In this section we analyze the production data of a tight oil well completed in Bakken formation. The well is hydraulically fractured consisting of 16 fracture stages and has been producing for nearly 3 years. Table 6.3 summarizes the available fluid and reservoir properties.

Table 6.3 Reservoir and fluid properties of well in Bakken Formation

Reservoir Type	Unknown	Permeability – Horizontal **(k_{hor})**	0.026 mD
Dominant Flow	Oil Phase	API Gravity	40 API
Multiphase flow in reservoir	No	Reservoir thickness **(h)**	19 ft.
Reservoir Pressure **(P_i)**	6800 psia	Matrix Porosity **(ϕ_m)**	0.09
Flowing BHP **(P_{wf})**	Varying	Total Compressibility **(c_t)**	1.726 x 10^{-5} psi^{-1}
Number of stages of fractures	16	Oil Formation Volume factor **(B_o)**	1.329
Length of horizontal well **(X_e)**	5600 ft.	Oil Viscosity (μ_o)	0.5643 cp

We make the same specialized plot of oil flow rate versus material balance time as shown in **Fig. 6.6** to identify different flow regions.

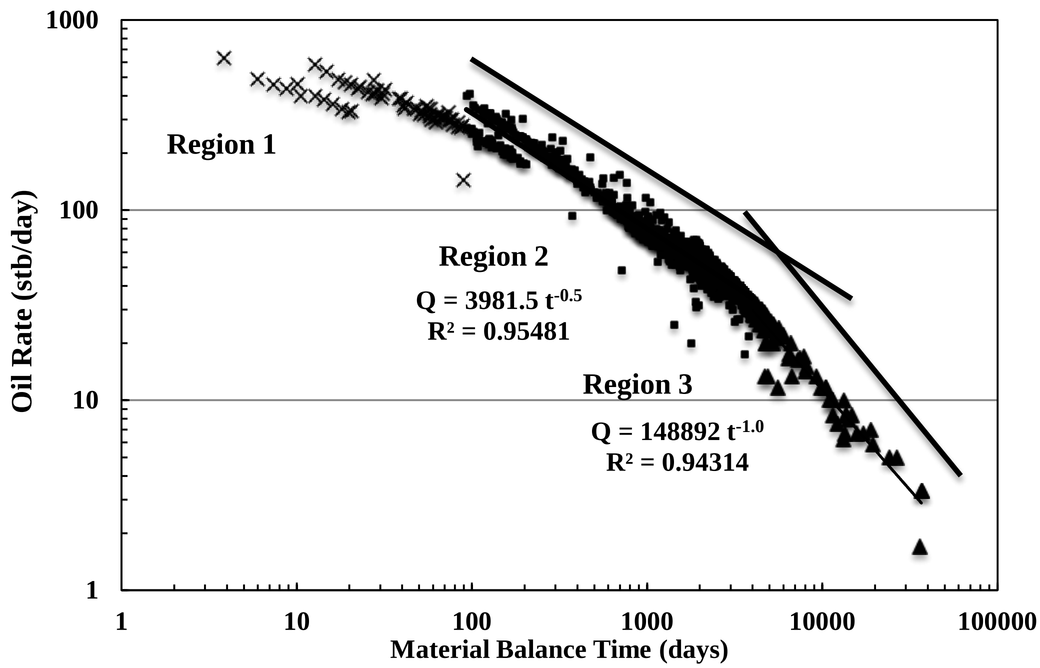

Fig. 6.6 – Log-log plot of daily oil rate versus calculated MBT of a Well in Bakken Formation.

In Fig. 6.6, we clearly see the linear transient flow region identified by a negative half-slope followed by a pseudosteady state regime identified by negative one slope. We analyze these two regions separately.

6.4.1 Analysis of Linear Transient Region

In Fig. 6.7, we make the plot of RNP versus square root of MBT of matrix transient region.

We substitute the value of m, determined in Fig. 6.7, in the analysis equation of dual porosity model and calculate the fracture-matrix interface area A_{cm}:

$$\sqrt{k_m}A_{cm} = \frac{125.11\, B\, \mu}{\sqrt{(\emptyset \mu c_t)_m}}\frac{1}{m}$$

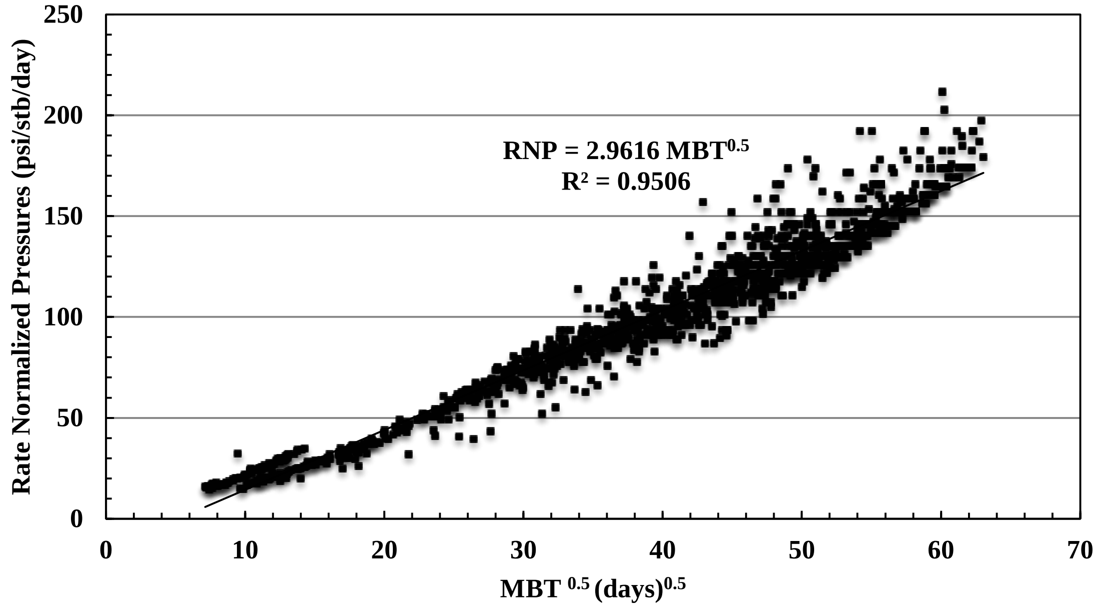

Fig. 6.7 – Plot of RNP versus square root of MBT of only transient region of the well completed in Bakken Formation

Slope of the line m = 2.96 psi / res bbl / day / day$^{0.5}$

$$A_{cm} = \frac{125.11 \times 1.329 \times 0.5643}{\sqrt{0.013}\sqrt{(0.09 \times 0.5643 \times 1.726 \times 10^{-5})}} \frac{1}{2.9616}$$

$$A_{cm} = 296{,}778.41 \text{ ft}^2$$

Using Eq. 3.11 to determine A_{cw}

$$A_{cw} = 2 \times X_e \times h$$

$$A_{cw} = 2 \times 5600 \times 19 = 212{,}800 \text{ ft}^2$$

Stimulated fracture half-length y_e is calculated to be

$$y_e = \frac{296{,}778.41 \times 312.5}{212{,}800}$$

$y_e = 435.82$ ft

The stimulated reservoir volume (SRV) $= 2 \times X_e \times h \times \phi_m \times y_e$ is calculated to be 8,346,824.6 ft^3 .

6.4.2 Analysis Of Boundary Dominated Flow

In Fig. 6.8, we plot the RNP versus MBT of the boundary-dominated flow region.

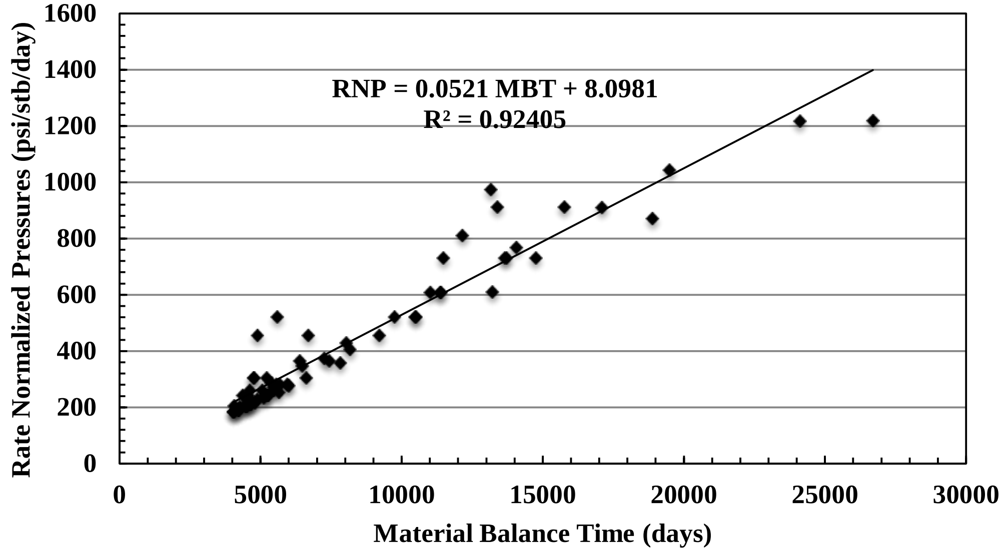

Fig. 6.8 – Specialized plot of RNP versus MBT for analyzing boundary dominated flow in Bakken Formation

Slope of the line $m_{ss} = 0.0521$ psi / STB / day / day

And $b_{ss} = 8.0981$ psi / STB / day

Using Eq.6.2

$$m_{ss} = \frac{5.615\ B_o}{A_{cw}\, y_e\, \phi_m\, c_t}$$

We also know that Stimulated Reservoir Volume $(SRV) = A_{cw}\, y_e\, \phi_m$

Therefore,

$$SRV = 5.615 \frac{B_o}{c_t} \frac{1}{m} = 5.615 \frac{1.329}{1.726 \times 10^{-5}} \frac{1}{0.0521} = 8{,}298{,}435.6 \text{ ft}^3$$

Now we use the intercept equation to determine the matrix permeability:

$$b_{ss} = \frac{36.96 \, \mu \, B_o \, L_f}{k_m \, N_f \, y_e \, h}$$

$$k_m = \frac{36.96 \, \mu \, B_o \, L_f}{b_{ss} \, N_f \, y_e \, h} = \frac{36.96 \times 0.5643 \times 1.329 \times 312.5}{8.098 \times 16 \times 435.82 \times 19} = 0.008 \text{ mD}$$

6.4.3 Summary of Results

The analysis results are summarized in Table 6.4.

Table 6.4 Unknown reservoir parameters obtained from the analysis of the matrix transient region and boundary dominated region of production data of the well completed in Bakken Formation

PARAMETER	VALUE
Slope of line for matrix region **m**	2.96 psi / res bbl / day / day$^{0.5}$
Slope of line for PSS region $\mathbf{m_{ss}}$	0.0521 psi / STB / day / day
Intercept of the line b_{ss} for PSS	8.0981 psi / STB / day
Permeability **k**	0.008 mDarcy (PSS Analysis)
	0.026 mDarcy (Well Tests)
Total Reservoir Area - $\mathbf{A_{cw}}$	212,800 sq.ft
Drainage Interface - $\mathbf{A_{cm}}$	309,502 sq.ft
Effective fracture half length - $\mathbf{y_e}$	454.5 ft.
Stimulated Reservoir Volume **SRV**	8,346,824.64 ft^3 (Matrix Analysis)
	8,298,435.6 ft^3 (Pseudo steady state Analysis)

The value of SRV obtained by analyzing the linear transient region is similar to that obtained by analyzing the PSS region. The value of permeability obtained by well testing and that obtained from our PSS analysis are different (See Table 6.4). This difference can be due to the heterogeneity of the reservoir.

CHAPTER VII
CONCLUSION AND RECOMMENDATIONS

7.1 CONCLUSIONS

The major findings of this work can be summarized as follows:

1. New equations have been developed for analyzing different regions of production data from tight reservoirs with induced hydraulic and reactivated natural fractures.
2. A procedure is proposed for determining the reservoir properties by using the hydrocarbon production data and the proposed equations.
3. We used the proposed equations to analyze the production data of two wells from Barnett shale. The results show that a dual porosity model is more appropriate than a triple porosity data for describing Barnett well data. Even if the micro-fractures are present in Barnett shale, their length scale should be less than the spacing between the hydraulic fractures.
4. New equations are developed to analyze boundary dominated (pseudosteady state) flow of a slightly compressible fluid in linear dual-porosity systems.
5. The pseudosteady state model proposed for boundary-dominated flow can be used in determining stimulated reservoir volume, minimum reservoir permeability. The proposed linear pseudo-steady state analysis complements the previously developed linear transient analysis.
6. We used the proposed PSS model to analyze the production data of two tight oil wells from Cardium and Bakken reservoirs. The results show that values of stimulated reservoir volume obtained from analysis of transient matrix flow and boundary dominated flow are very close for selected wells in both formations. The values of permeability are very close in Cardium well and relatively close for Bakken Well.

7.2 RECOMMENDATIONS

The following subjects remain the subject of future study:

1. The analysis equations were developed for the fully transient triple porosity model. Similar equations can be developed by considering the assumption of pseudosteady state matrix-fracture interflow assumption.
2. The analysis equations can be extended to include the skin effect.
3. The analysis equations for boundary dominated flow in triple porosity reservoirs can be developed.

REFERENCES

1. Abdassah, D. and Ershaghi, I. 1986. Triple-Porosity Systems for Representing Naturally Fractured Reservoirs. *SPE Form Eval* (April): 113 – 127. SPE-13409-PA.
2. Al-Ahmadi, H. A. 2010, A triple porosity model for fractured horizontal well. MSc. Dissertation, Texas A&M U., College Station, Texas.
3. Al-Ahmadi, H. A., Almarzooq, A. M. and Wattenbarger, R. A. 2010. Application of Linear Flow Analysis to Shale Gas Wells – Field Cases. Paper SPE 130370 presented at the 2010 Unconventional Gas Conference, Pittsburgh, Pennsylvania, 23 – 25 February.
4. Al-Ghamdi, A. and Ershaghi, I. 1996. Pressure Transient Analysis of Dually Fractured Reservoirs. *SPE J.* (March): 93 – 100. SPE-26959-PA.
5. Al-Hussainy, R., Ramey, H. J., Jr., and Crawford, P. B. 1966. The Flow of Real Gas Through Porous Media. *J. Pet Tech* (May): 624 – 636. SPE-1243A-PA
6. Anderson, D. M., Nobakht, M., Moghadam, S. and Mattar, L. 2010. Analysis of Production Data from Fractured Shale Gas Wells. Paper SPE 131787 presented at the SPE Unconventional Gas Conference, Pittsburgh, Pennsylvania, 23 – 25 February.
7. Barenblatt, G. I., Zhelto, I. P. and Kochina, I. N. 1960. Basic Concepts of the Theory of Seepage of Homogeneous Liquids in Fissured Rocks. *Journal of Applied Mathematical Mechanics* (USSR) **24** (5): 852 – 864.
8. Barrodale, I. and Roberts, F. D. K. 1974. Solution of an Overdetermined System of Equations in the l_1 Norm. *Communication of the ACM* **17** (6): 319 – 320.
9. Beckner, B.L., 1990, "Improved Modeling of Imbibition Matrix/Fracture Fluid Transfer in Double Porosity Simulators", PhD Dissertation at Stanford University.

10. Bello, R.O. 2009. Rate Transient Analysis in Shale Gas Reservoirs with Transient Linear Behavior. Ph.D. Dissertation, Texas A&M U., College Station, Texas.
11. Bello, R. O. and Wattenbarger, R. A. 2008. Rate Transient Analysis in Naturally Fractured Shale Gas Reservoirs. Paper SPE 114591 presented at the CIPC/SPE Gas Technology Symposium 2008 Joint Conference, Calgary, Alberta, Canada, 16 – 19 June.
12. Bello, R. O. and Wattenbarger, R. A. 2009. Modeling and Analysis of Shale Gas Production with a Skin Effect. Paper CIPC 2009-082 presented at the Canadian International Petroleum Conference, Calgary, Alberta, Canada, 16 – 18 June.
13. Bello, R. O. and Wattenbarger, R. A. 2010. Multi-stage Hydraulically Fractured Shale Gas Rate Transient Analysis. Paper SPE 126754 presented at the SPE North Africa Technical Conference and Exhibition held in Cairo, Egypt, 14 – 17 February.
14. Blasingame, T.A and Lee, W.J : "The Variable-Rate Reservoir Limits Testing", paper SPE 15028 presented at SPE Permian basin Oil & Gas Recovery Conference, Midland, March 13-14, 1986
15. Brown, M., Ozkan, E., Raghavan, R. and Kazemi, H. 2009. Practical Solutions for Pressure Transient Responses of Fractured Horizontal Wells in Unconventional Reservoirs. Paper SPE 125043 presented at the Annual Technical Conference and Exhibition, New Orleans, Louisiana, 4 – 7 October.
16. Bumb, A. C and McKee, C. R. 1988. Gas-Well Testing in the Pressure of Desorption for Coalbed Methane and Devonian Shale. *SPE Form Eval* (March): 179 - 185. SPE- 15227-P A.
17. Cheney, E.W. and Kincaid, R. D. 1985. Numerical Mathematics and Computing, 2nd edition. Monterey, California: Brooks/Cole Publishing Company.
18. de Swaan, O. A. 1976. Analytic Solutions for Determining Naturally

Fractured Reservoir Properties by Well Testing. *SPE J.* (June): 117 – 122. SPE-5346-PA.

19. Dreier, J. 2004. Pressure-Transient Analysis of Wells in Reservoirs with a Multiple Fracture Network. M.Sc. Thesis, Colorado School of Mines, Golden, Colorado.
20. Dreier, J., Ozkan, E. and Kazemi, H. 2004. New Analytical Pressure-Transient Models to Detect and Characterize Reservoirs with Multiple Fracture Systems. Paper SPE 92039 presented at the SPE International Petroleum Conference in Mexico, Puebla, Mexico, 8 – 9 November.
21. El-Banbi, A.H. 1998. Analysis of Tight Gas Wells. Ph.D. Dissertation, Texas A &M U., College Station, Texas.
22. Gale, J. F., Reed, R. M. and Holder, J. 2007. Natural Fractures in the Barnett Shale and Their Importance for Hydraulic Fracture Treatments. *AAPG Bulletin*. **91** (4): 603 – 622.
23. Jalali, Y. and Ershaghi, I. 1987. Pressure Transient Analysis of Heterogeneous Naturally Fractured Reservoirs. Paper SPE 16341 presented at the SPE California Regional Meeting, Ventura, California, 8 – 10 April.
24. Kazemi, H. 1969. Pressure Transient of Naturally Fractured Reservoirs with Uniform Fracture Distribution. *SPE J.* (December):451– 462. SPE-2156A-PA.
25. Liu, C. Q. 1981. Exact Solution for the Compressible Flow Equations through a Medium with Triple-Porosity. *Applied Mathematics and Mechanics* **2** (4): 457 – 462.
26. Liu, C. Q. 1983. Exact Solution of Unsteady Axisymmetrical Two-Dimensional Flow through Triple Porous Media. *Applied Mathematics and Mechanics* **4** (5): 717 – 724.
27. Liu, J. C., Bodvarsson, G. S. and Wu, Y. S. 2003. Analysis of Flow Behavior in Fractured Lithophysal Reservoirs. *Journal of Contaminant Hydrology* **62-63**: 189 – 211.

28. Mayerhofer, M. J., Lolon, E. P., Youngblood, J. E. and Heinze, J. R. 2006. Integration of Microseismic Fracture Mapping Results with Numerical Fracture Network Production Modeling in the Barnett Shale. Paper SPE 102103 presented at the Annual Technical Conference and Exhibition, San Antonio, Texas, 24 – 27 September.
29. Medeiros, F., Ozkan, E. and Kazemi, H. 2008. Productivity and Drainage Area of Fractured Horizontal Wells in Tight Gas Reservoirs. *SPE Res Eval & Eng* (October): 902 – 911. SPE-108110-PA.
30. Nelson, R. A. 2001. Geologic Analysis of Naturally Fractured Reservoirs, 2nd edition. Woburn, Massachusetts: Butterworth-Heinemann.
31. Ordonez, A., Penuela, G. et al., Dec. 2001, “Recent Advances in Naturally Fractured Reservoir Modeling”, published in CT&F, Vol. 2.
32. Ozkan, E., Brown, M., Raghavan, R. and Kazemi, H. 2009. Comparison of Fractured Horizontal-Well Performance in Conventional and Unconventional Reservoirs. Paper SPE 121290 presented at the SPE Western Regional Meeting, San Jose, California, 24 – 26 March.
33. Ozkan, E., Ohaeri, U. and Raghavan, R. 1987. Unsteady Flow to a Well Produced at a Constant Pressure in Fractured Reservoir. *SPE Form Eval* (June): 186 - 200. SPE- 9902-P A.
34. Palacio, J.C., and Blasingame, T.A. Decline-Curve Analysis With Type Curves – Analysis of Gas Well Production Data. Paper SPE 25909 presented at the 1993 SPE Rocky Mountain Regional/Low Permeability Reservoir Symposium, Denver, Colorabo, 12 - 14 April.
35. Saidi, A.M., Nov. 1983, “Simulation of Naturally Fractured Reservoirs”, paper SPE 12270 presented at the Seventh SPE Symposium on Reservoir Simulation held in San Francisco, CA.
36. Song, B., Economides, M.J., and Ehlig-Economides, C.A. 2009. Design of Multiple Transverse Fracture Horizontal Wells in Shale Gas Reservoirs. Paper SPE 140555 presented at the 2011 SPE Hydraulic Fracturing

Technology Conference, Woodlands, TX, 24 - 26 January.

37. Stehfest, H. 1970. Algorithm 358 – Numerical Inversion of Laplace Transforms. *Communication of the ACM* **13** (1): 47 – 49.
38. Warren, J. E. and Root, P. J. 1963. The Behavior of Naturally Fractured Reservoirs. *SPE J.* (September): 245 – 255. SPE-426-PA.
39. Wattenbarger, R.A. 2007. Some Reservoir Performance Aspects of Unconventional Gas Production. Private Conference Presentation, Lake Louise, Alberta, Canada.
40. Wu, Y. S., Liu, H. H. and Bodvarsson, G. S. 2004. A Triple-Continuum Approach for Modeling Flow and Transport Processes in Fractured Rock. *Journal of Contaminant Hydrology* **73**: 145 – 179.

NOMENCLATURE

A_{cm} = Total matrix/micro-fracture surface drainage area, ft^2

A_{cw} = well-face cross-sectional area to flow, ft^2

c_t = total compressibility, psi^{-1}

$f_f(s)$ = fracture function for matrix-micro-fracture fluid transfer

$f(s)$ = fracture function for micro-fracture-macro-fracture fluid transfer

h = matrix block thickness, ft.

k_f = permeability of micro-fracture, md

k_F = permeability of macro-fracture, md

k_m = permeability of matrix block, md

$\mathcal{L}^{-1}$= inverse Laplace operator

L_f = micro fracture spacing, ft.

L_F = macro fracture spacing, ft.

m_r = slope of region

$m(pi)$= gas pseudo pressure at initial conditions, psi^2 /cp

$m(pwf)$= gas pseudo pressure at well-bore, psi^2 /cp

N_p = cumulative oil production

n_{fxe} = number of micro fractures in the direction of well length

n_{fye} = number of macro fractures in the direction of macro-fracture length

Pi = pressure of reservoir at initial conditions, psi

P_{wf} = pressure of reservoir at well-bore, psi

q_{DL} = dimensionless flow rate

q_g = gas rate, MScf/day

q_o = oil rate produced from one fracture, m^3/s

Q_o = daily oil rate, STB/day

s = laplace space variable

t = time, days

$\bar{t}$ = material balance time, days

t_{dac} =dimensionless time

T = absolute temperature, ^0R

x_D = dimensionless distance along micro-fracture spacing

X_e = length of horizontal well, ft.

y_{De} = dimensioless length of reservoir

y_e = macro-fracture half-length , ft.

z_D = dimensionless distance along macro-fracture spacing

Greek Symbols

Ø = porosity, fraction

μ = viscosity of a gas , cp

σ_i = shape factor, 1/ft^2

ω_i = storativity ratio

λ_{Ac} = dimensionless interporosity flow

Subscript

f = micro-fracture

F = macro-fracture

m = matrix

i = f,F, &m

ss = Pseudo steady state

o = oil

g = gas

APPENDIX A

TRANSIENT LINEAR TRIPLE POROSITY ANALYTICAL SOLUTIONS

The rate solutions in fractured linear reservoirs is derived by Laplace transformation which enables us to reduce the second-order partial differential flow equations to a second order ordinary differential equation in Laplace domain. Stehfest algorithm (Stehfest 1970) is then used to easily invert the Laplace domain solution to time domain.

The differential equation in Laplace domain that describes the main flow in linear reservoir system is given by

$$\frac{\partial^2 p_{DLF}}{\partial y_D^2} - sf(s)\overline{p_{DLF}} = 0 \qquad (A-1)$$

A-1 Linear Flow Solutions for Fractured Linear Reservoirs (Dual Porosity System)

El-Banbi (1998) developed the first linear flow solutions for dual porosity system in fractured linear reservoirs. In Laplace domain, Eq. A-2 relates the constant rate and constant pressure solutions at the well bore

$$\overline{p_{wDL}} \times \overline{q_{DL}} = \frac{1}{s^2} \qquad (A-2)$$

Therefore, the solution for constant pressure case (El-Banbi 1998) is

$$\frac{1}{\overline{q_{Dl}}} = \frac{2\pi s}{\sqrt{sf(s)}}\left[\frac{1 + e^{-2\sqrt{sf(s)}y_{De}}}{1 - e^{-2\sqrt{sf(s)}y_{De}}}\right] \qquad (A-3)$$

A-2 Analytical Solutions for Triple Porosity System in Linear Reservoirs

Al-Ahmadi (2010) developed the analytical solutions for triple porosity system in linear reservoirs. The three contagious media include: macro-fractures, micro-fractures and matrix. The fluid flow is assumed to be sequential i.e. matrix to micro-fractures and micro-fractures to macro-fractures. The schematic of the Al-Ahmadi (2010) triple porosity model is shown in Fig. A-1.

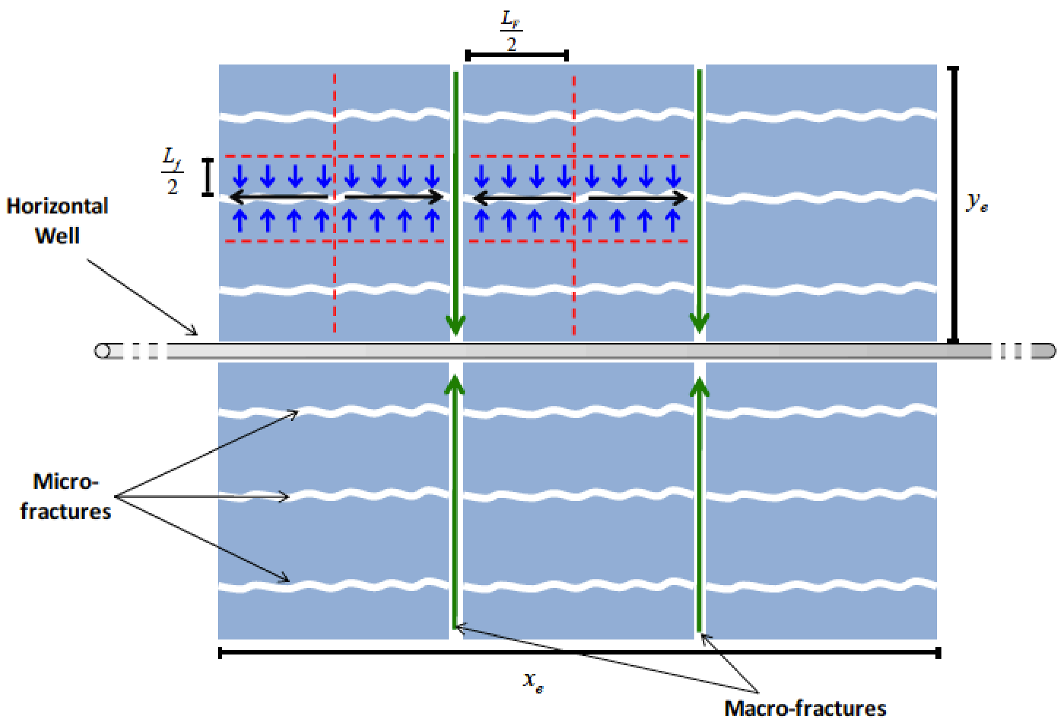

Fig. A-4 – Top View of a horizontal Well in a triple porosity system. Red dotted lines indicated virtual no flow boundaries. Arrows indicate direction of the flow (Al-Ahmadi 2010).

A-3 Summary of Equations used in developing Analytical Solutions

This section presents the summary of analytical equations used by Al-Ahmadi to develop the analytical solutions. For details of the derivation of the solutions, refer to Al-Ahmadi dissertation (2010).

A-3.1 Matrix Equation

Matrix equation under transient condition is given by

$$\frac{k_m}{\mu}\frac{\partial^2 p_m}{\partial z^2} = (\varphi V c_t)_m \frac{\partial p_m}{\partial t} \qquad (\mathrm{A}-4)$$

$$\frac{\partial^2 p_m}{\partial z^2} = \frac{(\varphi V \mu c_t)_m}{k_m}\frac{\partial p_m}{\partial t} \qquad (\mathrm{A}-5)$$

A-3.2 Micro-fracture Equation

Micro-fracture equation under transient condition is given by

$$\frac{k_f}{\mu}\frac{\partial^2 p_f}{\partial x^2} + q_{source,m} = (\varphi V c_t)_f \frac{\partial p_f}{\partial t} \qquad (\mathrm{A}-6)$$

Where $q_{source,m}$ is a source term of flow term from matrix to micro-fracture, given by

$$q_{source,m} = -{}^{1}\!/_{L_f}\,\frac{k_m}{\mu}\frac{\partial p_m}{\partial z}\bigg|_{z={}^{L_f}\!/_{2}} \qquad (\mathrm{A}-7)$$

Thus, the final form of micro-fractures equation is

$$\frac{\partial^2 p_f}{\partial x^2} = \frac{(\varphi V \mu c_t)_f}{k_f}\frac{\partial p_f}{\partial t} + {}^{1}\!/_{L_f}\,\frac{k_m}{k_f}\frac{\partial p_m}{\partial z}\bigg|_{z={}^{L_f}\!/_{2}} \qquad (\mathrm{A}-8)$$

A-3.3 Macro-fracture Equation

Macro-fracture equation under transient condition is given by

$$\frac{k_F}{\mu}\frac{\partial^2 p_F}{\partial y^2} + q_{source,f} = (\varphi V c_t)_F \frac{\partial p_F}{\partial t} \qquad (\mathrm{A}-9)$$

Where $q_{source,m}$ is a source term of flow term from micro-fractures to macro-fracture, given by

$$q_{source,f} = -\,{}^{1}\!/_{L_F}\frac{k_f}{\mu}\frac{\partial p_f}{\partial x}\bigg|_{x={}^{L_F}\!/_{2}} \qquad (\mathrm{A}-10)$$

A-3.4 Initial and Boundary conditions

Matrix

Initial Condition:

$$p_m(z,0) = p_i$$

Inner Boundary:

$$\frac{\partial p_m}{\partial z} = 0 \qquad @\, z = 0$$

Outer boundary

$$p_m = p_f \qquad @\, z = \frac{L_f}{2}$$

Micro-fracture

Initial Condition:

$$p_f(x,0) = p_i$$

Inner Boundary:

$$\frac{\partial p_f}{\partial x} = 0 \qquad @\, x = 0$$

Outer Boundary:

$$p_f = p_F \qquad @\, x = \frac{L_F}{2}$$

Macro-fracture

Initial Condition:

$$p_F(y,0) = p_i$$

Inner Boundary:

$$q = -\frac{k_F A_{cw}}{\mu}\frac{\partial p_F}{\partial y}\Big|_{y=0}$$

Outer Boundary:

$$\frac{\partial p_F}{\partial y} = 0 \qquad @\, y = y_e$$

A-3.5 System Dimensionless Equations

Equations presented in Appendix A-3.3 can be converted to dimensionless equations using dimensional variables defined in Chapter 3 and dimensionless boundary conditions.

Matrix:

$$\frac{\partial^2 p_{DLm}}{\partial z_D^2} = \frac{3\omega_m}{\lambda_{Ac,fm}}\frac{\partial p_{DLm}}{\partial t_{DAc}} \qquad (\mathrm{A}-11)$$

Micro-fracture:

$$\frac{\partial^2 p_{DLf}}{\partial x_D^2} = \frac{3\omega_f}{\lambda_{Ac,Ff}}\frac{\partial p_{DLf}}{\partial t_{DAc}} + \frac{\lambda_{Ac,fm}}{\lambda_{Ac,Ff}}\frac{\partial p_{DLm}}{\partial z_D}\Big|_{z_{D=1}} \qquad (\mathrm{A}-12)$$

Macro-fracture:

$$\frac{\partial^2 p_{DLF}}{\partial y_D^2} = \omega_F\frac{\partial p_{DLF}}{\partial t_{DAc}} + \frac{\lambda_{Ac,Ff}}{3}\frac{\partial p_{DLf}}{\partial x_D}\Big|_{x_{D=1}} \qquad (\mathrm{A}-13)$$

A-3.6 Laplace Transformation

The differential equations presented in Appendix A-3.5 are transformed into Laplace domain.

Matrix Equation

$$\overline{p_{DLm}} = \frac{\overline{p_{DLf}}}{cosh\left(\sqrt{\frac{3s\omega_m}{\lambda_{Ac,fm}}}\right)} cosh\left(\sqrt{\frac{3s\omega_m}{\lambda_{Ac,fm}}} z_D\right) \qquad (A-14)$$

Micro-fracture Equation

$$\overline{p_{DLf}} = \frac{\overline{p_{DLF}}}{cosh\left(\sqrt{sf_f(s)}\right)} cosh\left(\sqrt{sf_f(s)} x_D\right) \qquad (A-15)$$

Macro-fracture Equation

$$\frac{\partial \overline{p_{DLF}}}{\partial {y_D}^2} = \omega_F \, s \, \overline{p_{DLF}} + \frac{\lambda_{Ac,Ff}}{3} \frac{\partial \overline{p_{DLf}}}{\partial {x_D}^2}\bigg|_{x_D=1} \qquad (A-16)$$

Differentiating Eq. A-15 and Replacing in Eq. A-16, the solution becomes

$$\frac{\partial^2 \overline{p_{DLF}}}{\partial y_D^2} - s\overline{p_{DLF}}\left[\omega_F + \frac{\lambda_{Ac,Ff}\sqrt{sf_f(s)}tanh\left(\sqrt{sf_f(s)}\right)}{3s}\right] = 0 \qquad (A-17)$$

In short form

$$\frac{\partial^2 \overline{p_{DLF}}}{\partial y_D^2} - sf(s)\overline{p_{DLF}} = 0 \qquad (A-18)$$

Where $f(s)$ is Al-Ahmadi’s transfer function for the fully transient case is given by

$$f(s) = \omega_F + \frac{\lambda_{AcFf}}{3s}\sqrt{sf_f(s)}\,\tanh\sqrt{sf_f(s)} \qquad (A-19)$$

Where $f_f(s)$ is given as

$$f_f(s) = \frac{3\omega_f}{\lambda_{AcFf}} + \frac{\lambda_{Acfm}}{s\lambda_{AcFf}}\sqrt{\frac{3s\omega_m}{\lambda_{Acfm}}}\tanh\sqrt{\frac{3s\omega_m}{\lambda_{Acfm}}} \qquad (A-20)$$

APPENDIX B

DEVELOPMENT OF ANALYSIS EQUATIONS

In this section, the analysis equations for the linear triple porosity model are derived. Al-Ahmadi's transfer function "$f(s)$" is further simplified to develop analysis equation for each region. The fluid transfer is assumed to be under transient flow. Al-Ahmadi's transfer function $f(s)$ for the transient case is given by

$$f(s) = \omega_F + \frac{\lambda_{AcFf}}{3s}\sqrt{sf_f(s)}\tanh\sqrt{sf_f(s)} \qquad (B-1)$$

Where $f_f(s)$ is given as

$$f_f(s) = \frac{3\omega_f}{\lambda_{AcFf}} + \frac{\lambda_{Acfm}}{s\lambda_{AcFf}}\sqrt{\frac{3s\omega_m}{\lambda_{Acfm}}}\tanh\sqrt{\frac{3s\omega_m}{\lambda_{Acfm}}} \qquad (B-2)$$

Eq. B-1 and B-2 are replaced in El-Banbi (1998) Laplace solution developed for linear reservoirs. The equation for constant pressure inner boundary, closed outer boundary (slab matrix) developed by El-Banbi is given as

$$\frac{1}{\overline{q_{Dl}}} = \frac{2\pi s}{\sqrt{sf(s)}}\left[\frac{1+e^{-2\sqrt{sf(s)}y_{De}}}{1-e^{-2\sqrt{sf(s)}y_{De}}}\right] \qquad (B-3)$$

Using

$$\coth(x) = \frac{e^{2x}+1}{e^{2x}-1} \qquad (B-4)$$

Eq. B-3 can be written as

$$\frac{1}{\overline{q_{Dl}}} = \frac{2\pi s}{\sqrt{sf(s)}}\coth\left(\sqrt{sf(s)}y_{De}\right) \qquad (B-5)$$

Further simplifying the Eq. B-1, B-2 and B-5, we obtain the analysis equation for each individual regions observed on the log-log plot of dimensionless flow rate versus dimensionless time.

B-1 REGION 1

This region represents flow at early time scale in the macro-fractures only. Using Eq. B-5

$$\frac{1}{q_{Dl}} = \frac{2\pi s}{\sqrt{sf(s)}} \coth\left(\sqrt{sf(s)}y_{De}\right) \qquad (B-5)$$

For early time, the value is s is larger (Since t and s are inversely related)

Approximately for x > 3, $\coth\ (x) = 1$

Therefore for

$\coth\left(\sqrt{sf(s)}y_{De}\right) = 1$ When $\sqrt{sf(s)}y_{De} > 3$

Eq. B-5 can be written as

$$\frac{1}{q_{Dl}} = \frac{2\pi s}{\sqrt{sf(s)}} \qquad (B-6)$$

Here $f(s)$ is given as

$$f(s) = \omega_F + \frac{\lambda_{AcFf}}{3s}\sqrt{sf_f(s)}\tanh\sqrt{sf_f(s)} \qquad (B-1)$$

Where $f_f(s)$ is given as

$$f_f(s) = \frac{3\omega_f}{\lambda_{AcFf}} + \frac{\lambda_{Acfm}}{s\lambda_{AcFf}}\sqrt{\frac{3s\omega_m}{\lambda_{Acfm}}}\tanh\sqrt{\frac{3s\omega_m}{\lambda_{Acfm}}} \qquad (B-2)$$

For early time scales (higher values of s) considering fracture depletion only, we can assume in Eq. B-1

$$\omega_F \ggg \frac{\lambda_{AcFf}}{3s}\sqrt{sf_f(s)}\tanh\sqrt{sf_f(s)}$$

Therefore Eq. B-1 can be simplified into

$$f(s) = \omega_F \qquad (B-7)$$

Replacing B-7 in Eq. B-6 we obtain,

$$\frac{1}{\overline{q_{Dl}}} = \frac{2\pi s}{\sqrt{s\omega_F}} \qquad (B-8)$$

or

$$\overline{q_{Dl}} = \frac{1}{2\pi\sqrt{s}}\sqrt{\omega_F} \qquad (B-9)$$

Eq. B-9 can be converted from Laplace space to time domain by applying inverse Laplace on both sides. The inverted equation is given as

$$q_{Dl} = \frac{1}{2\pi\sqrt{\pi t_{dac}}}\sqrt{\omega_F} \qquad (B-10)$$

Using definition of dimensionless parameters defined, Eq. B-10 is converted to obtain the analysis equation for Region 1,

$$\sqrt{k_F}A_{cw} = \frac{1262T}{\sqrt{(\emptyset\mu c_t)_f}}\frac{1}{m_1} \qquad (B-11)$$

Where m_1 is the slope obtained by plotting $\frac{m(p_i)-m(p_{wf})}{q_g}$ against $\sqrt{t}$

B-2 Region 2

This region is observed during when bilinear flow occurs between macro fracture and micro fracture. Using Eq. B-5

$$\frac{1}{\overline{q_{Dl}}} = \frac{2\pi s}{\sqrt{sf(s)}}\coth\left(\sqrt{sf(s)}y_{De}\right) \qquad (B-5)$$

This region also occurs at early time scale, as the permeability of macro-fractures is very high. For early time, the value is s is larger (Since t and s are inversely related)

Approximately for x > 3, coth $(x) = 1$

Therefore,

$\coth\left(\sqrt{sf(s)}y_{De}\right) = 1$ When $\sqrt{sf(s)}y_{De} > 3$

Eq. B-5 can be written as,

$$\frac{1}{q_{Dl}} = \frac{2\pi s}{\sqrt{sf(s)}} \qquad (\mathrm{B}-6)$$

Here $f(s)$ is given as

$$f(s) = \omega_F + \frac{\lambda_{AcFf}}{3s}\sqrt{sf_f(s)}\tanh\sqrt{sf_f(s)} \qquad (\mathrm{B}-1)$$

Where $f_f(s)$ is given as,

$$f_f(s) = \frac{3\omega_f}{\lambda_{AcFf}} + \frac{\lambda_{Acfm}}{s\lambda_{AcFf}}\sqrt{\frac{3s\omega_m}{\lambda_{Acfm}}}\tanh\sqrt{\frac{3s\omega_m}{\lambda_{Acfm}}} \qquad (\mathrm{B}-2)$$

During the production from macro-fractures and micro-fractures, the flow from matrix is assumed to be zero. Therefore Eq. B-2 can be simplified into,

$$f_f(s) = \frac{3\omega_f}{\lambda_{AcFf}} \qquad (\mathrm{B}-12)$$

Replacing Eq. B-12 in Eq. B-1,

$$f(s) = \omega_F + \frac{\lambda_{AcFf}}{3s}\sqrt{s\frac{3\omega_f}{\lambda_{AcFf}}}\tanh\sqrt{s\frac{3\omega_f}{\lambda_{AcFf}}} \qquad (\mathrm{B}-13)$$

Since,

tanh(x) ≈ 1, for x > 3

Therefore for higher values of s

$\tanh\sqrt{sf_f(s)} \approx 1$, for $\sqrt{sf_f(s)} > 3$

Therefore Eq. B-13 can be written as

$$f(s) = \omega_F + \frac{\lambda_{AcFf}}{3s}\sqrt{sf_f(s)} \qquad (\mathrm{B}-14)$$

For bilinear flow from micro-fractures and macro-fractures, we can assume storativity of macro-fractures doesn't play a significant role. Therefore,

$$\omega_F \lll\lll \frac{\lambda_{AcFf}}{3s}\sqrt{sf_f(s)}$$

Eq. B-14 can be written as

$$f(s) = \frac{\lambda_{AcFf}}{3s}\sqrt{sf_f(s)} \qquad (\mathrm{B}-15)$$

Replacing Eq. B-15 in B-6

$$\frac{1}{\overline{\overline{q_{Dl}}}} = \frac{2\pi s}{\overline{\overline{\sqrt{s\frac{\lambda_{AcFf}}{3s}\sqrt{sf_f(s)}}}}} \qquad (\mathrm{B}-16)$$

Substituting the value of Eq. B-12 in Eq. B-16

$$\frac{1}{\overline{\overline{q_{Dl}}}} = \frac{2\pi s}{\overline{\overline{\sqrt{s\frac{\lambda_{AcFf}}{3s}\sqrt{s\frac{3\omega_f}{\lambda_{AcFf}}}}}}} \qquad (\mathrm{B}-17)$$

Simplifying B-17 to obtain analytical solution for Region 2 in Laplace space

$$\overline{q_{Dl}} = \frac{1}{2\pi}\sqrt[4]{\frac{\lambda_{AcFf}\omega_f}{3}}\,s^{-0.75} \qquad (\mathrm{B}-18)$$

Inverting Eq. B-18 in real time, using Laplace inversion. The analytical solution for Region 2 is obtained as

$$q_{Dl} = \frac{1}{10.1332}\sqrt[4]{\frac{\lambda_{AcFf}\omega_f}{t_{dac}}} \qquad (\mathrm{B}-19)$$

Using definition of dimensionless parameters defined, Eq. B-19 is converted to obtain the analysis equation for Region 2,

$$\sqrt{k_F}A_{cw} = \frac{4070T}{\sqrt[4]{\sigma_F k_f(\emptyset\mu c_t)_f}}\frac{1}{m_2} \qquad (\mathrm{B}-20)$$

Where m_2 is the slope obtained by plotting $\frac{m(p_i)-m(p_{wf})}{q_g}$ against $\sqrt[4]{t}$.

B-3 Region 3

This region represents the transient linear flow occurring in the micro-fracture only. Using Eq. B-5

$$\frac{1}{q_{Dl}} = \frac{2\pi s}{\sqrt{sf(s)}} \coth\left(\sqrt{sf(s)}y_{De}\right) \qquad (\mathrm{B}-5)$$

Here $f(s)$ is given as

$$f(s) = \omega_F + \frac{\lambda_{AcFf}}{3s}\sqrt{sf_f(s)}\tanh\sqrt{sf_f(s)} \qquad (\mathrm{B}-1)$$

Where $f_f(s)$ is given as

$$f_f(s) = \frac{3\omega_f}{\lambda_{AcFf}} + \frac{\lambda_{Acfm}}{s\lambda_{AcFf}}\sqrt{\frac{3s\omega_m}{\lambda_{Acfm}}}\tanh\sqrt{\frac{3s\omega_m}{\lambda_{Acfm}}} \qquad (\mathrm{B}-2)$$

In Region 3 flow is from micro-fractures only, therefore storativity and interporosity of matrix blocks can be neglected.

$$\omega_f \ggg\ggg\ggg\ggg\ggg \frac{\lambda_{Acfm}}{3s}\sqrt{\frac{3s\omega_m}{\lambda_{Acfm}}}\tanh\sqrt{\frac{3s\omega_m}{\lambda_{Acfm}}}$$

Eq. B-2 can be written as

$$f_f(s) = \frac{3\omega_f}{\lambda_{AcFf}} \qquad (\mathrm{B}-21)$$

Since,

$\tanh(x) \approx 1$, for $x > 3$

Therefore for higher values of s

$\tanh\sqrt{sf_f(s)} \approx 1$, for $\sqrt{sf_f(s)} > 3$

Eq. B-1 becomes,

$$f(s) = \omega_F + \frac{\lambda_{AcFf}}{3s}\sqrt{sf_f(s)} \qquad (\mathrm{B}-22)$$

Similarly for Region 3, storativity of macro-fracture is also neglected.

$$\omega_F \lll\lll< \frac{\lambda_{AcFf}}{3s}\sqrt{sf_f(s)}$$

Eq. B-22 becomes

$$f(s) = \frac{\lambda_{AcFf}}{3s}\sqrt{sf_f(s)} \qquad (\mathrm{B}-23)$$

Consider Eq. B-5

$$\frac{1}{\overline{q_{Dl}}} = \frac{2\pi s}{\overline{\sqrt{sf(s)}}} \coth\left(\sqrt{sf(s)}y_{De}\right) \qquad (\mathrm{B}-5)$$

Taylor series expansion of coth (x) is given as

$$\coth x = \frac{1}{x} + \frac{x}{3} - \frac{x^3}{45} + \cdots \ldots \ldots \ldots \ldots \ldots \ldots ..$$

Assume

$$\coth x \approx \frac{1}{x}$$

$$\coth\sqrt{sf(s)}\, y_{De} \approx \frac{1}{\overline{\sqrt{sf(s)y_{De}}}}$$

Replacing in Eq. B-5

$$\frac{1}{\overline{q_{Dl}}} = \frac{2\pi s}{sf(s)y_{De}} \qquad (\mathrm{B}-24)$$

Substituting Eq. B-23 in Eq. B-24, we obtain,

$$\frac{1}{\overline{q_{Dl}}} = \frac{2\pi s}{s\frac{\lambda_{AcFf}}{3s}\sqrt{sf_f(s)}y_{De}} \qquad (B-25)$$

Substituting Eq. B-21 in Eq. B-25

$$\frac{1}{\overline{q_{Dl}}} = \frac{2\pi s}{s\frac{\lambda_{AcFf}}{3s}\sqrt{s\frac{3\omega_f}{\lambda_{AcFf}}}y_{De}} \qquad (B-26)$$

Simplifying Eq. B-26, we obtain the analytical solution in Laplace space,

$$\overline{q_{Dl}} = \frac{1}{2\pi}\sqrt{\frac{\lambda_{AcFf}\omega_f}{3s}}y_{De} \qquad (B-27)$$

Inverting Eq. B-27 to real time, we obtain

$$q_{DL} = \frac{1}{2\pi\sqrt{\pi t_{dac}}}\sqrt{\frac{\lambda_{AcFf}\omega_f}{3}}y_{De} \qquad (B-28)$$

Using definition of dimensionless parameters defined, Eq. B-28 is converted to obtain the analysis equation for Region 3,

$$\sqrt{\sigma_F}y_e\sqrt{k_f}A_{cw} = \frac{2182T}{\sqrt{(\emptyset\mu c_t)_f}}\frac{1}{m_3} \qquad (B-29)$$

Where m_3 is the slope obtained if we plot $\frac{m(p_i)-m(p_{wf})}{q_g}$ against $\sqrt{t}$

B-4 Region 4

This region represents transient bi-linear flow between micro-fractures and macro-fractures. Using Eq. B-5

$$\frac{1}{\overline{q_{Dl}}} = \frac{2\pi s}{\sqrt{sf(s)}}\coth\left(\sqrt{sf(s)}y_{De}\right) \qquad (B-5)$$

Here $f(s)$ is given as

$$f(s) = \omega_F + \frac{\lambda_{AcFf}}{3s}\sqrt{sf_f(s)}\tanh\sqrt{sf_f(s)} \qquad (B-1)$$

Where $f_f(s)$ is given as

$$f_f(s) = \frac{3\omega_f}{\lambda_{AcFf}} + \frac{\lambda_{Acfm}}{s\lambda_{AcFf}}\sqrt{\frac{3s\omega_m}{\lambda_{Acfm}}}\tanh\sqrt{\frac{3s\omega_m}{\lambda_{Acfm}}} \qquad (\mathrm{B}-2)$$

During bilinear flow between micro fracture and matrix, storativity of micro-fractures doesn't play a significant role hence it can be neglected in Eq. B-2.

$$\omega_f <<<< \frac{\lambda_{Acfm}}{3s}\sqrt{\frac{3s\omega_m}{\lambda_{Acfm}}}\tanh\sqrt{\frac{3s\omega_m}{\lambda_{Acfm}}}$$

Eq. B-2 becomes,

$$f_f(s) = \frac{\lambda_{Acfm}}{s\lambda_{AcFf}}\sqrt{\frac{3s\omega_m}{\lambda_{Acfm}}}\tanh\sqrt{\frac{3s\omega_m}{\lambda_{Acfm}}} \qquad (\mathrm{B}-30)$$

Assuming

$$\sqrt{\frac{3s\omega_m}{\lambda_{Acfm}}} > 3$$

Approximately for x>3, $\tanh \mathrm{x} = 1$

Therefore

$$\tanh\sqrt{\frac{3s\omega_m}{\lambda_{Acfm}}} \approx 1$$

Eq. B-30 becomes,

$$f_f(s) = \frac{\lambda_{Acfm}}{s\lambda_{AcFf}}\sqrt{\frac{3s\omega_m}{\lambda_{Acfm}}} \qquad (\mathrm{B}-31)$$

For Region 4, storativity of macro-fractures can also be neglected in Eq. B-1

$$\omega_F \lll\ll \frac{\lambda_{AcFf}}{3s}\sqrt{sf_f(s)}\tanh\sqrt{sf_f(s)}$$

In order to simplify the equation, we assume $\tanh\sqrt{sf_f(s)} \approx 1$

Eq. B-31 can be written as,

$$f(s) = \frac{\lambda_{AcFf}}{3s}\sqrt{sf_f(s)} \tag{B − 32}$$

Now consider equation B-5

$$\frac{1}{\overline{q_{Dl}}} = \frac{2\pi s}{\sqrt{sf(s)}} \coth\left(\sqrt{sf(s)}y_{De}\right) \tag{B − 5}$$

Taylor series expansion of coth (x) is given as

$$\coth x = \frac{1}{x} + \frac{x}{3} - \frac{x^3}{45} + \cdots \ldots \ldots \ldots \ldots \ldots \ldots ..$$

Assume

$$\coth x \approx \frac{1}{x}$$

$$\coth \sqrt{sf(s)}\, y_{De} \approx \frac{1}{\sqrt{sf(s)y_{De}}}$$

Eq. B-5 becomes,

$$\frac{1}{\overline{q_{Dl}}} = \frac{2\pi s}{sf(s)y_{De}} \tag{B − 36}$$

Replacing $f(s)$ from Eq. B-32 in Eq. B-36,

$$\frac{1}{\overline{q_{Dl}}} = \frac{2\pi s}{s\,\frac{\lambda_{AcFf}}{3s}\sqrt{sf_f(s)}y_{De}} \tag{B − 37}$$

Replacing $f_f(s)$ from Eq. B-31 in Eq. B-37,

$$\frac{1}{\overline{q_{Dl}}} = \frac{2\pi s}{s\,\frac{\lambda_{AcFf}}{3s}\sqrt{s\,\frac{3}{\lambda_{AcFf}}\left(\frac{\lambda_{Acfm}}{3s}\sqrt{\frac{3s\omega_m}{\lambda_{Acfm}}}\right)}y_{De}} \tag{B − 38}$$

Simplifying Eq. B-38,

$$\overline{q_{Dl}} = \frac{1}{2\pi}\frac{\sqrt{\lambda_{AcFf}}\sqrt[4]{\lambda_{Acfm}\omega_m}}{\sqrt[3]{3s}}y_{De} \qquad (B-39)$$

Inverting Eq. B-39 to real time using Laplace inversion,

$$q_{Dl} = \frac{1}{2\pi}\frac{\sqrt{\lambda_{AcFf}}\sqrt[4]{\lambda_{Acfm}\omega_m}}{\sqrt[3]{3}}y_{De}\frac{\Gamma(0.75)}{t_{dac}{}^{0.25}} \qquad (B-40)$$

Further simplifying Eq. B-40, we obtain the analytical solution for Region 4

$$q_{Dl} = \frac{1}{17.31}\sqrt{\lambda_{AcFf}}\sqrt[4]{\frac{\lambda_{Acfm}\omega_m}{t_{dac}}}y_{De} \qquad (B-41)$$

Using definition of dimensionless parameters defined, Eq. B-41 is converted to obtain the analysis equation for Region 4,

$$\sqrt{\sigma_F}y_e\sqrt{k_f}A_{cw} = \frac{6943T}{\sqrt[4]{\sigma_f k_m(\emptyset\mu c_t)_m}}\frac{1}{m_4} \qquad (B-42)$$

Where m_4 is the slope obtained if we plot $\frac{m(p_i)-m(p_{wf})}{q_g}$ against $\sqrt[4]{t}$

B-5 Region 5

This region represents the transient linear case when the transient linear response is primarily from the drainage of the matrix. Using Eq. B-5

$$\frac{1}{\overline{q_{Dl}}} = \frac{2\pi s}{\sqrt{sf(s)}}\coth\left(\sqrt{sf(s)}y_{De}\right) \qquad (B-5)$$

Here $f(s)$ is given as

$$f(s) = \omega_F + \frac{\lambda_{AcFf}}{3s}\sqrt{sf_f(s)}\tanh\sqrt{sf_f(s)} \qquad (B-1)$$

Where $f_f(s)$ is given as

$$f_f(s) = \frac{3\omega_f}{\lambda_{AcFf}} + \frac{\lambda_{Acfm}}{s\lambda_{AcFf}}\sqrt{\frac{3s\omega_m}{\lambda_{Acfm}}}\tanh\sqrt{\frac{3s\omega_m}{\lambda_{Acfm}}} \qquad (B-2)$$

Consider Eq. B-2, during linear flow in the matrix

$$\omega_f <<<<<<< \frac{\lambda_{Acfm}}{3s}\sqrt{\frac{3s\omega_m}{\lambda_{Acfm}}}\tanh\sqrt{\frac{3s\omega_m}{\lambda_{Acfm}}}$$

Eq. B-2 can be reduced to

$$f_f(s) = \frac{\lambda_{Acfm}}{s\lambda_{AcFf}}\sqrt{\frac{3s\omega_m}{\lambda_{Acfm}}}\tanh\sqrt{\frac{3s\omega_m}{\lambda_{Acfm}}} \qquad (\mathrm{B}-43)$$

In order to simplify Eq. B-43, we assume that $\omega_m > \lambda_{Acfm}$ as the storativity of matrix is very high as compared to the interporosity flow parameter. Hence,

$$\sqrt{\frac{3s\omega_m}{\lambda_{Acfm}}} > 3$$

Therefore,

$$\tanh\sqrt{\frac{3s\omega_m}{\lambda_{Acfm}}} \approx 1$$

Eq. B-43 can be written as

$$f_f(s) = \frac{\lambda_{Acfm}}{s\lambda_{AcFf}}\sqrt{\frac{3s\omega_m}{\lambda_{Acfm}}} \qquad (\mathrm{B}-44)$$

Substituting Eq. B-44 in Eq. B-1 and neglecting ω_F,

$$f(s) = \frac{\lambda_{AcFf}}{3s}\sqrt{s\frac{\lambda_{Acfm}}{s\lambda_{AcFf}}\sqrt{\frac{3s\omega_m}{\lambda_{Acfm}}}}\tanh\sqrt{s\frac{\lambda_{Acfm}}{s\lambda_{AcFf}}\sqrt{\frac{3s\omega_m}{\lambda_{Acfm}}}} \qquad (\mathrm{B}-45)$$

Or

$$f(s) = \frac{\lambda_{AcFf}}{3s}\sqrt[4]{\frac{3s\quad\lambda_{Acfm}}{\lambda_{AcFf}{}^2}\omega_m}\tanh\sqrt[4]{\frac{3s\quad\lambda_{Acfm}}{\lambda_{AcFf}{}^2}\omega_m} \qquad (\mathrm{B}-46)$$

Since $k_f \gg k_m$, therefore $\lambda_{AcFf} >> \lambda_{Acfm}$, the assumption of $\frac{3s \ \ \lambda_{Acfm}}{\lambda_{AcFf}{}^2}\omega_m > 3$ is not valid.

Using Taylor approximation

$\tanh(x) \approx x$

Eq. B-46 can be simplified as

$$f(s) = \frac{\lambda_{AcFf}}{3s}\sqrt{\frac{3s \ \ \lambda_{Acfm}}{\lambda_{AcFf}{}^2}\omega_m} \qquad (\mathrm{B}-47)$$

Or

$$f(s) = \sqrt{\frac{\lambda_{Acfm}}{3\ s}\omega_m} \qquad (\mathrm{B}-48)$$

Now consider equation B-5

$$\frac{1}{\overline{\overline{q_{Dl}}}} = \frac{2\pi s}{\sqrt{sf(s)}} \coth\left(\sqrt{sf(s)}y_{De}\right) \qquad (\mathrm{B}-5)$$

Taylor series expansion of coth (x) is given as

$$\coth x = \frac{1}{x} + \frac{x}{3} - \frac{x^3}{45} + \cdots \ldots \ldots \ldots \ldots \ldots \ldots$$

Assume

$$\coth x \approx \frac{1}{x}$$

$$\coth\sqrt{sf(s)}\, y_{De} \approx \frac{1}{\overline{\sqrt{sf(s)}y_{De}}}$$

Eq. B-5 becomes,

$$\frac{1}{\overline{\overline{q_{Dl}}}} = \frac{2\pi s}{sf(s)y_{De}} \qquad (\mathrm{B}-49)$$

Substituting Eq. B-48 in Eq. B-49

$$\frac{1}{\overline{q_{Dl}}} = \frac{2\pi s}{s\sqrt{\frac{\lambda_{Acfm}}{3\,s}\omega_m y_{De}}} \quad (\mathrm{B}-50)$$

Or

$$q_{Dl} = \frac{1}{2\pi\sqrt{s}}\sqrt{\frac{\lambda_{Acfm}\omega_m}{3}}y_{De} \quad (\mathrm{B}-51)$$

Inverting Eq. B-51 to real time using Laplace inversion,

$$q_{Dl} = \frac{1}{2\pi\sqrt{\pi t_{dac}}}\sqrt{\frac{\lambda_{Acfm}\omega_m}{3}}y_{De} \quad (\mathrm{B}-52)$$

Using definition of dimensionless parameters defined, Eq. B-52 is converted to obtain the analysis equation for Region 5,

$$\sqrt{\sigma_f}y_e\sqrt{k_m}A_{cw} = \frac{2182T}{\sqrt{(\emptyset\mu c_t)_m}}\frac{1}{m_5} \quad (\mathrm{B}-53)$$

Where m_5 is the slope obtained if we plot $\frac{m(p_i)-m(p_{wf})}{q_g}$ against $\sqrt{t}$